

ABSTRACT

Title of Thesis: DIELECTRIC STUDIES OF LIQUID
CRYSTAL NANOCOMPOSITES AND
NANOMATERIAL SYSTEMS.

Ravindra Kempaiah, Master of Science, 2016

Thesis Directed By: Assistant Professor, Dr. Zhihong Nie, and
Department of Chemistry and Biochemistry

Liquid crystals (LCs) have revolutionized the display and communication technologies. Doping of LCs with inorganic nanoparticles such as carbon nanotubes, gold nanoparticles and ferroelectric nanoparticles have garnered the interest of research community as they aid in improving the electro-optic performance. In this thesis, we examine a hybrid nanocomposite comprising of 5CB liquid crystal and block copolymer functionalized barium titanate ferroelectric nanoparticles. This hybrid system exhibits a giant soft-memory effect. Here, spontaneous polarization of ferroelectric nanoparticles couples synergistically with the radially aligned BCP chains to create nanoscopic domains that can be rotated electromechanically and locked in space even after the removal of the applied electric field. We also present the latest results from the dielectric and spectroscopic study of field assisted alignment of gold nanorods.

DIELECTRIC STUDIES OF LIQUID CRYSTAL NANOCOMPOSITES
AND
NANOMATERIAL SYSTEMS.

By
Ravindra Kempaiah

Thesis submitted to the Faculty of the Graduate School of the
University of Maryland, College Park, in partial fulfillment
of the requirements for the degree of
Master of Science

2016

Advisory Committee

Assistant Professor Dr. Zhihong Nie, Chair

Assistant Professor Dr. Efrain Rodriguez

Professor Dr. Jeffery Davis

© Copyright by
Ravindra Kempaiah
2016

Acknowledgements

I am honored by the fact that I have been a member and research student at the University of Maryland and I have immensely benefitted by the research expertise that abounds the reputed labs of this university.

As I move forward in my academic career, I would like to thank few people who have played pivotal role in my research so far and have helped me shape this thesis:

Prof. Dr. Zhihong Nie, my supervisor, for accepting me into his research group, the support and responsibility of my Master's thesis and for giving me orientation in experimental research by devoting his time and resources.

Dr. Rajratan Basu , for guiding me through this work, for allowing me to work in his lab and for giving me an opportunity to learn the fundamentals of liquid crystals science.

Dr. Jake Fontana, for his collaborative work and always encouraging me. I have immensely benefitted by his knowledge and experience.

My fellow lab mates Yijing Liu, Cheng Lin Yi, and Yang Yang for their assistance in the lab and fruitful discussions leading to successful experimental results.

Contents

ABSTRACT	i
Acknowledgements	ii
Contents	iii
List of Figures.....	v
Chapter 1 Introduction.....	1
1.1 Different polarization mechanisms	2
1.2 Broadband Dielectric Spectroscopy.....	6
Chapter 2 Dielectric Studies of Liquid crystal Nanocomposites.....	8
2.1 Liquid Crystal Materials	8
2.2 Liquid Crystal Structure and Phases.....	10
2.3 Nanocomposites and Doping with Nanoparticles.....	13
2.4 Motivation and Hypotheses.....	15
2.5 Materials and characterization methods.....	18
2.5.1 Materials.....	18
2.5.2 Surface Functionalization and Nanocomposite Preparation	19
2.5.3 Dielectric Characterization.....	21
2.6 Experimental Findings and Discussions.....	24
Chapter 3 Dielectric Spectroscopy of Gold Nanorods	43
3.1 Materials and Characterization Methods	44
3.2 Dielectric Anisotropy and Spectroscopy Measurements	47
3.3 Quantitative Measurement of Dielectric Anisotropy	50
3.4 Dielectric Spectroscopy	53
Chapter 4 Perspective and Future Work.....	57
4.1 Ionic Conductivity in Doped LCs	57
4.2 Ferroelectric Polymers in LCs	58
4.3 Conclusions.....	60
Appendix A X-ray Diffraction pattern of BaTiO ₃	61
Appendix B Dielectric Spectroscopy setup.....	62

References 63

List of Figures

Figure 1-1 : Dielectric material	2
Figure 1-2: Various polarization mechanisms. (Courtesy: Dr. Raj Basu, USNA) ...	3
Figure 1-3: (a) Debye relaxation wherein the frequency dependence of $\epsilon'(w)$ and $\epsilon''(w)$ are plotted. (b) geometrical representation of dissipation factor in a relaxation process.....	5
Figure 1-4: Different polarization mechanisms in dielectric materials	7
Figure 2-1(a) order of phases as the temperature is changed (b) Molecular structure of 5CB. (c) Graphical representation of rod-like anisotropic mesogen.	9
Figure 2-2: Different phases of thermotropic LC systems	12
Figure 2-3: (a) and (b) usage of FNPs in high permittivity dielectrics and relaxor materials with enhanced capacitance [Ref 16, 17].....	15
Figure 2-4: Graphical representation of the following materials (a) Barium titanate FNP, (b) Amphiphilic block copolymer, (c) 5CB rod-like molecule, (d) 5CB molecules randomly arranged in isotropic phase, (e) BaTiO ₃ suspended in isotropic phase of 5CB showing alignment along the particle interface.	20
Figure 2-5: Polarized optical microscopy images of BaTiO ₃ FNP doped 5CB under cross-polarizers. (a) and (b) show minimal texture, while (c) has very minimal aggregates but (d) has large aggregates that could short the cell.....	21
Figure 2-6: (a) schematic of the circuitry of the dielectric measurement setup at USNA. (b) Automatic liquid crystal tester (ALCT) equipment connected to a programmable precision stage and LabVIEW interface. (Courtesy: Dr. Raj Basu, US Naval Academy).	23
Figure 2-7: (a) programmable microscope hot and cold stage with LC cell. (b) Schematic of the LC cells coated with ITO from Instec Inc.....	24
Figure 2-8: Dielectric constant of pure 5CB, 5CB doped with BaTiO ₃ FNPs and polymer modified BaTiO ₃ FNPs at 0.275 wt %. Dielectric constant is plotted against applied RMS field ($f= 1$ KHz) and in nematic phase of LCs (25°C).	27
Figure 2-9: Dielectric hysteresis of pure 5CB (black), pure PEO45-b-PS670-SH polymer (purple) doped in 5CB, 5CB/ bare BaTiO ₃ composite (red), polymer functionalized BaTiO ₃ FNPs (blue and green) as a function of applied electric field in isotropic phase ($T= 42^\circ\text{C}$).	29
Figure 2-10: Schematic representation of enhanced pseudonematic domains as a result of polymer functionalization of FNPs and the subsequent increase in the dielectric anisotropy.....	31

Figure 2-11: (a) When there is no applied field across the LC cell, the mesogens are randomly oriented (b) we see that upon the application of AC field across the LC cell, pseudonematic domains mechanically rotate BaTiO ₃ FNPs in the direction of the field. The density of mesogens is greater along the poles. This remnant polarization leads to giant soft-memory.	32
Figure 2-12: Non-volatility of pseudonematic domains in the isotropic phase of 5CB. The dielectric constant maintains a constant value over a period of 3 days.....	33
Figure 2-13: Dielectric hysteresis area of PEO ₄₅ -b-PS ₆₇₀ -SH polymer functionalized BaTiO ₃ nanocomposite as a function of concentration of dopants. Inset shows the dielectric hysteresis for various polymers that were used to functionalize BaTiO ₃ and dope 5CB LC.....	35
Figure 2-14: (a) Molecular structure of PEO ₄₅ -b-PS ₆₇₀ -SH BCP. (b) Schematic illustrating the π - π stacking interaction between 5CB mesogens and benzene rings of polystyrene units.	37
Figure 2-15: Scanning Electron Microscopy images of the pure BaTiO ₃ and PEO ₄₅ -b-PS ₆₇₀ -SH BCP functionalized BaTiO ₃ FNP's. From the inset (a) and (c), we can infer that clusters and random aggregates are prevalent. Functionalized samples as shown in (b) and (d) provides evidence of uniform colloidal dispersion.....	40
Figure 3-1: AuNRs with their respective LSPR peak and transmission electron microscopy (TEM) images.	45
Figure 3-2: (a-c) Sequence of steps involved in phase transferring of AuNRs.	46
Figure 3-3: (a) Schematic of the custom designed ITO cell with dimensions. (b) Actual image of the cell used.....	48
Figure 3-4: Schematic illustrating the induced dipole in AuNRs within a ITO cell, under the applied electric field.....	49
Figure 3-5 : Change in dielectric constant as a function of applied electric field for 5 μ cell has been plotted. Dielectric constant increases with voltage.	51
Figure 3-6: Dielectric anisotropy as a function of aspect ratio of the nanorods.....	52
Figure 3-7: (left) Real component indicating the storage factor. (Right) Imaginary component of complex dielectric constant indicating the loss factor.	54
Figure 3-8: Dielectric relaxation spectra of AuNRs dispersed in toluene. One can observe the distinct peak from the toluene chemical structure in both real and imaginary components.	55
Figure 3-9: Dielectric relaxation spectra of pure R.I oil as a function of frequency in a 5 μ m cell.....	56
Figure 4-1: Ionic conductivity of LC when doped with functionalized AuNPs.....	58

Figure 4-2: Hysteresis observed in PVDF doped 5CB in isotropic phase.....	59
Figure 0-1: XRD spectra indicating the single phase of BaTiO ₃ nanoparticles (Courtesy of U.S Nanomaterials Research Inc.).....	61
Figure 0-1: Keysight E4980A and E4982A broadband frequency spectrometers.	62

Chapter 1

Introduction

Materials that conduct electrical current under the influence of an electric field are called conductors. Materials whose internal charges do not flow freely under the application of electric field are called insulators. According to the band theory of solids, in a conductor, the charges can be excited to electronic states where they can move freely (conduction band) and this energy difference is often referred to as 'band gap'. Most insulators have large band gaps. A dielectric material is an insulator that can be polarized by the application of an electric field. Here, the electrons are bound to the nucleus and have limited movement and when an external field is applied, the nucleus of the atoms are attracted to the negative terminal and the electrons are pulled towards the positive terminal and tend to align in equilibrium position. These charges separated by a small distance constitute a 'dipole' and the process is known as 'polarization' (P). The term 'dielectric' is often used to indicate the energy storing capacity of the material and dielectrics are an efficient supporter of electrostatic fields. The extent to which a substance concentrates the electrostatic lines of flux can be quantified by "*Dielectric constant*" ($\epsilon = \epsilon_r \epsilon_0$) or in other words, the response of charge-free sample to an applied electric field.¹ In corollary, all dielectrics are insulators but not all insulators are dielectrics. The polarizability and structural arrangement dictates the behavior of dielectrics (Figure 1-1). The built-up polarization in dielectrics take a certain finite time (τ) before reaching its maximum value. This time-dependent dynamics is characteristic to each material and is termed as 'dielectric relaxation'.

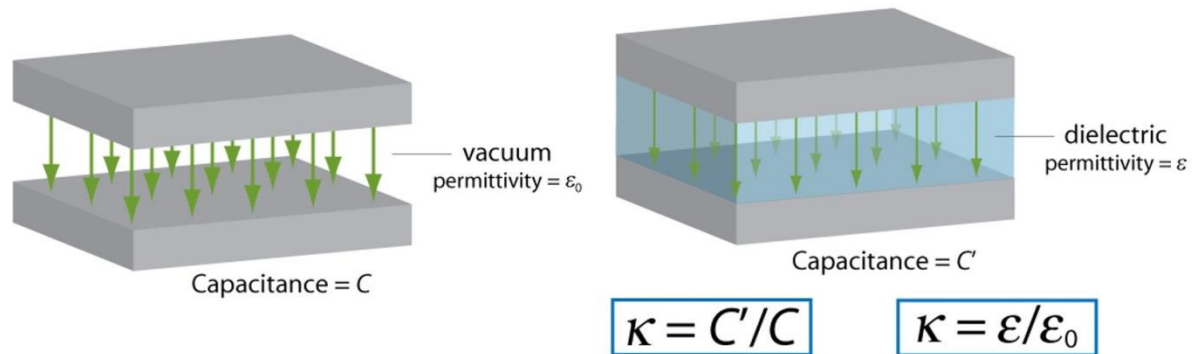


Figure 1-1 : Dielectric material

1.1 Different polarization mechanisms

Dielectric relaxation processes are studied based on the frequency range within which it is most active.²

1. Electronic polarization (α_e): Fast response, τ is small.

When an electric field is applied to an atom, positively charged nucleus displaces in the direction of the field and electron cloud in the opposite direction. This resonant process as a result of interplay between electric and restoration forces leading to an equilibrium occurs because of within an atom and the equilibrium displacement is proportional to the applied magnetic field. This is mostly observed in monoatomic gases and only at high enough optical frequencies (10^{15} Hz).

2. Ionic polarization (α_i): Slow response. This is a resonant process that occurs in a molecule comprising of charged atoms/ions. These ionic components get displaced under the applied field resulting in a net dipole moment.

3. Orientation or dipolar polarization (α_d): Slower response.

Certain molecules (e.g., CH_3Cl , HCl , and H_2O) carry inherent dipole moment and in the absence of any field, molecular dipoles are oriented randomly and cancel their moments. However, in the presence of electric field, these dipoles orient themselves in the direction of the field and the resulting net dipole is very large. The intrinsic frequency of the dipoles dictates the relaxation time. Also, the thermal perturbation and immediate chemical surrounding play a key role in the net resultant dipole.

4. Space charge polarization (α_s): very slow response. τ is large.

It is a combination of ionic conductivity, interfacial and space charge relaxation. At low frequencies, the ionic conductivity dominates and hence, the losses are introduced.

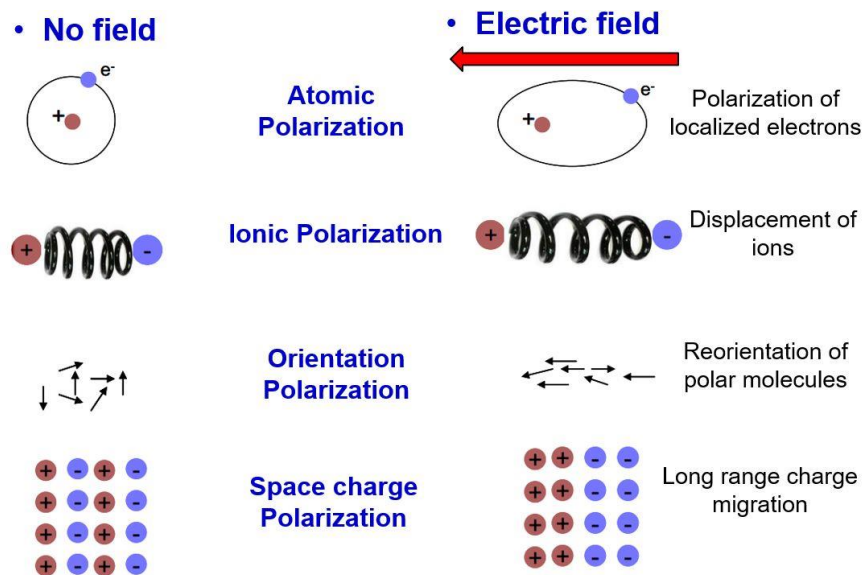


Figure 1-2: Various polarization mechanisms. (Courtesy: Dr. Raj Basu, USNA)

It is important to understand the frequency dependence of polarization and the dominant modes of relaxation for various frequency regimes. Relaxation time (τ) indicates

the mobility of molecules. As stated earlier, it is the time required for dipoles to become oriented in an electric field. Under solid and liquid conditions, the molecules are in condensed state and have limited freedom to move when an electric field is applied. The constant collision of molecules cause friction and with time τ , the molecules slowly approach the equilibrium polarization state/orientation.³ This buildup of polarization over time can be described by an equation (Equation 1), where $P(t)$ is the instant polarization at time t and P_{∞} is the built up polarization at $t = \infty$.

$$P(t) = P_{\infty} \left(1 - e^{-\frac{t}{\tau}}\right) \quad \text{(Equation 1-1)}$$

When the applied field is turned off, the molecules revert back to random orientation. Relaxation frequency (τ_f) can also defined as the inverse of relaxation time and at low frequencies below the τ_f , the dipoles keep up with the alternating electric field variations. Based on the exponential law quoted above, the real and imaginary components of dielectric constant can be deduced. The real/in-phase component can be written as,

$$\varepsilon' = \varepsilon_{\infty} + \frac{\Delta\varepsilon}{1+(\omega\tau)^2} \quad \text{(Equation 1-2)}$$

The out-of-phase (imaginary) component of the dielectric constant is,

$$\varepsilon'' = \varepsilon_{\infty} + \frac{\Delta\varepsilon}{1+(\omega\tau)^2} (\omega\tau) \quad \text{(Equation 1-3)}$$

Here, the ω is the frequency of the applied AC field and $\Delta\varepsilon = \varepsilon_0 - \varepsilon_{\infty}$ is the dielectric relaxation strength for an individual process. The dielectric strength at infinite

frequency is represented as ε_∞ and the static dielectric strength is given by ε_0 . The complex dielectric constant (ε^*) of a material then takes the form,

$$\varepsilon^*(\omega) = \varepsilon' - j\varepsilon'' \quad \text{(Equation 1-4)}$$

Here, the real component, $\varepsilon'(\omega)$ is the relative permittivity and represents the material's ability to store electric field energy and the imaginary part, $\varepsilon''(\omega)$ is the dielectric loss and gives us information about the energy loss of that material in a relaxation process.⁴

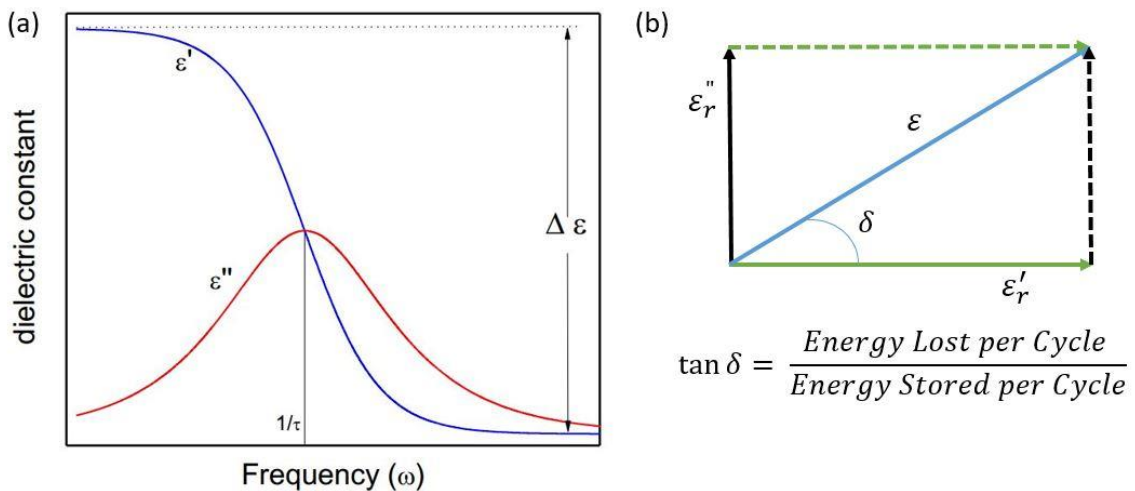


Figure 1-3: (a) Debye relaxation wherein the frequency dependence of $\varepsilon'(\omega)$ and $\varepsilon''(\omega)$ are plotted. (b) geometrical representation of dissipation factor in a relaxation process.

The dissipation factor described in Figure 1-3 is a measure of effectiveness of a dielectric material. In an ideal dielectric, the current leads the voltage by an angle of 90° , but in the case of a commercial dielectric, the current doesn't exactly leads the voltage by 90° , it leads by some other angle lesser than 90° and as a result, the electric displacement

in a dielectric will have a phase lag. To put it simply, the dielectric loss angle (Figure 1-3b) will be greater for a non-ideal dielectric. Now, we have some basic understanding of the dielectric materials, I will provide an introduction to the dielectric spectroscopy measurement technique used in my studies.

1.2 Broadband Dielectric Spectroscopy

Molecular dynamics can be studied by various techniques such as,

1. **Relaxation:** *Dielectric relaxation*, Nuclear Magnetic Resonance (NMR)
2. **Scattering:** Quasi-elastic light scattering, Neutron scattering
3. **Spectroscopy:** UV-Vis, IR, time-resolved fluorescence depolarization

Broadband dielectric spectroscopy is a powerful method for the study of interaction of electromagnetic waves with matter in the frequency domain of 10^{-6} Hz to 10^{12} Hz.⁵ In this extended dynamic range, molecular and collective dipolar fluctuations, charge transport and polarization effects occur and these phenomenon determine the overall dielectric response of a material. The graphical representation of dielectric dispersion in the frequency domain has been presented in Figure 1-4. At low frequencies, all of the polarization modes (electronic, ionic, dipolar and space charge) can keep up with the frequency.² Above 10^7 Hz, space charge mode can't keep up and that the dipolar mode is most active in the 10^9 - 10^{12} Hz window and that is indicated by a huge dip in the curve in

Figure 1-4. Subsequent downward gradient or fluctuations are attributed to the dominant modes in the frequency regime.

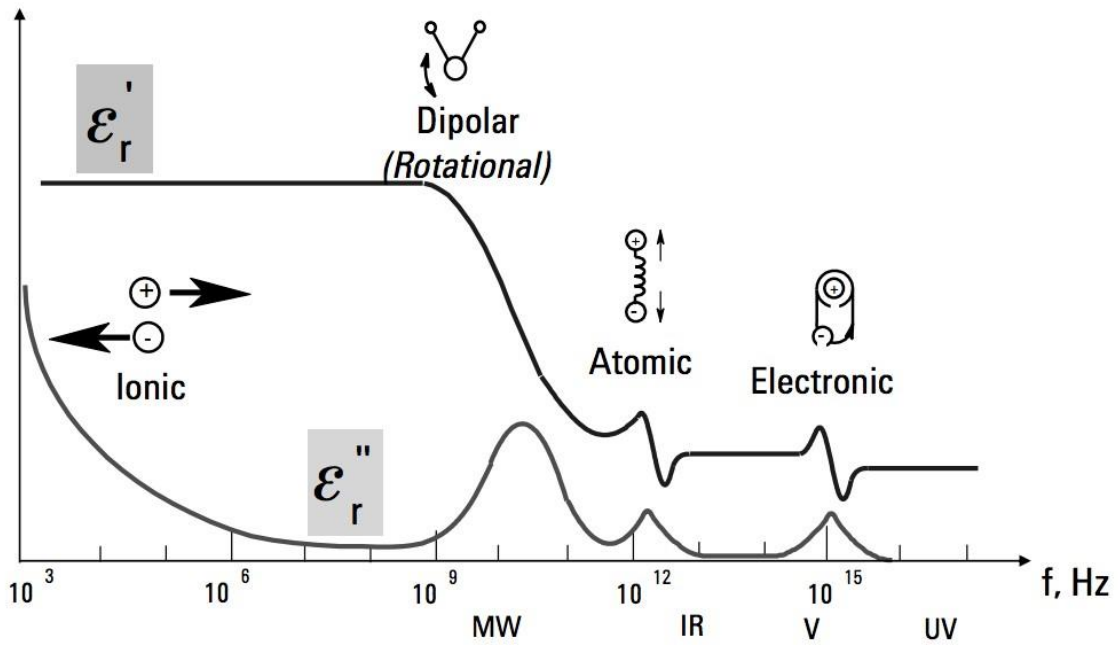


Figure 1-4: Different polarization mechanisms in dielectric materials

To span this large frequency range, normally two slightly different measurement instruments will be used. From 10^6 - 10^7 Hz, lumped circuit method which involve a parallel plate capacitor-type cells was used and for frequencies greater 10^7 Hz, distributed circuit methods with high resolution was used. More details about the specific instruments would be highlighted in the subsequent chapters.

Chapter 2

Dielectric Studies of Liquid crystal Nanocomposites

This chapter is largely adapted from the paper: [*Appl. Phys. Lett.* 108, 083105 \(2016\)](#)

Here in this chapter, we detail the experimental results of ferroelectric nanoparticle doped liquid crystal nanocomposites and the ‘soft-memory’ effect. Doping of liquid crystals (LCs) with nanoparticles, quantum dots and other nanomaterials have become a common method for improving their optical, magnetic, and physical properties.^{6,7} These enhanced properties could lead to various applications and researchers are studying them to understand different aspects such as electro-optical, dielectric, memory effects, self-assembly and phase behavior.^{8,9} However, doping ferroelectric nanoparticles (FNPs) in LCs is rarely reported in literature.¹⁰ Long-range forces between these nanoparticles and interplay of elastic forces of LCs produces interesting colloidal properties. We found that dielectric studies of FNPs in LC matrix in isotropic phase exhibits enhanced dielectric anisotropy and introduces ferroelectric behavior. We begin with introduction to LC systems and the doping methodologies and then move onto the detailed study.

2.1 Liquid Crystal Materials

Liquid crystal is a state of matter that is intermediate between the crystalline solid and the liquid phases i.e., it may flow like a conventional liquid, but have the molecules in the liquid have positional and/or orientational arrangement as shown in Figure 2-1a.

LCs were first discovered back in 1888 by an Austrian scientist, Friedrich Reinitzer when he tried to extract cholesteryl benzoate from carrots.¹¹

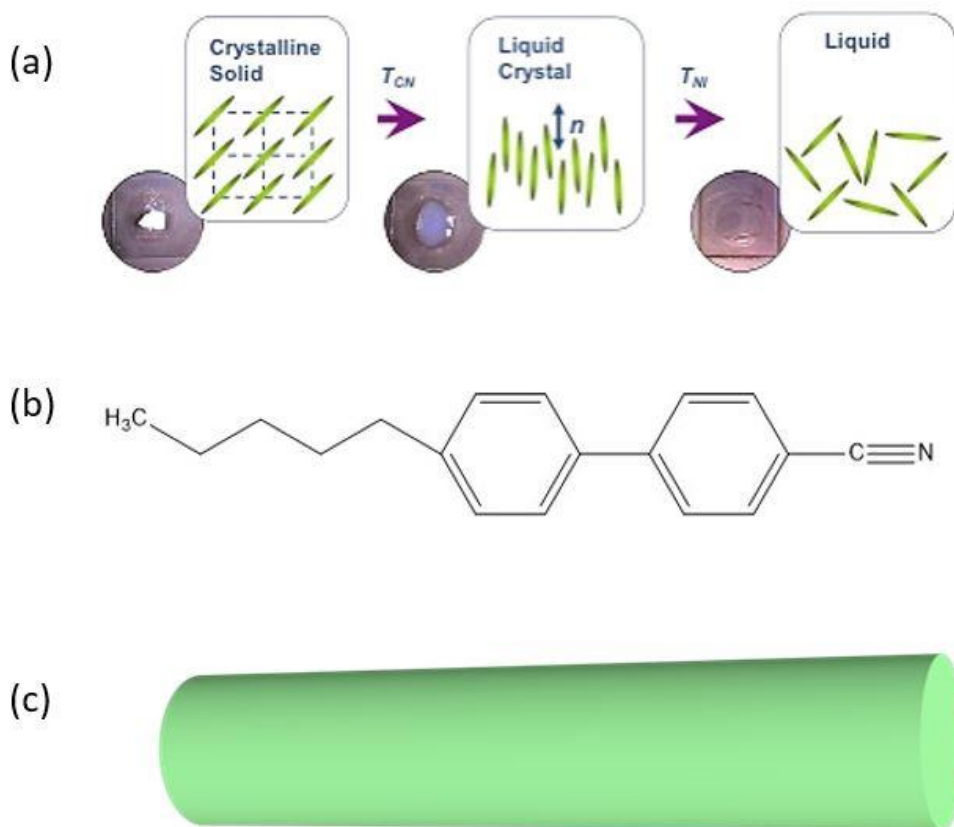


Figure 2-1(a) order of phases as the temperature is changed (b) Molecular structure of 5CB. (c) Graphical representation of rod-like anisotropic mesogen.

Later, collaborative studies conducted by Otto Lehmann, Von Zepharovich along with Reinitzer found that cholesteryl benzoate (LC monomer) exhibited (i) two distinct melting points (145.5°C and 178.5°C), (ii) reflected circularly polarized light and (iii) rotate

the polarization of light passing through them. The real breakthrough in LC research came about when Hans Keller synthesized a LC monomer that had a nematic phase at room temperature, N-(4-Methoxybenzylidene)-4-butylaniline (MBBA). The commercial application of LCs for displays took off when George Gray at the University of Hull synthesized low melting cyanobiphenyls that was stable over wide range of temperature.¹² The structure of most commonly used cyanobiphenyl, 4-Cyano-4'-pentylbiphenyl (5CB) has been shown in Figure 2-1.

2.2 Liquid Crystal Structure and Phases.

LC molecules are typically formed by a combination of aromatic rings attached to aliphatic chains/tails, as shown in Figure 2-1. The aromatic ring provides elastic moduli of solids whereas the aliphatic tail provides the fluidity to the LC molecules. As a result, the molecules (mesogens) are anisotropic in nature with aspect ratio ranging from 3 to 10, and their mechanical, electric and optical properties also exhibit anisotropic behavior. The average direction of the long axes of the molecules is called the director n .

There are two major categories of LC molecules:

1. Lyotropic LCs, whose mesophase formation is dependent on concentration and the solvent. Eg., lipids, fatty acids.
2. Thermotropic LCs, whose mesophase is temperature (T) dependent. This class of LC systems have a large repository of LC molecules.

Nobel laureate Pierre-Gilles de Gennes and G. Friedel did extensive studies and they classified the LC molecules based on the order and symmetry of the phases. Presented below is the most-widely accepted method of classification.

1. ***Nematic phase*** (from the Greek word Nematos meaning “thread”):

This phase of LC is characterized by molecules that do not have positional order (center of mass of each molecule is randomly placed) but orient along the same direction (the director). Molecules align parallel to each other and have long-range interaction, Figure 2-2.

2. ***Smectic phase*** (from the Green work Smectos meaning “soap”):

In this mesophase, the LC molecules show a degree of translational order and tend to align in layers or planes. The molecular motion is restricted to these planes. Because of the enhanced order, they have slightly ‘solid-like’ behavior. There are few distinct sub-phases within smectic category. Smectic-A mesophase has director perpendicular to the smectic plane and with no positional order within the planes. Smectic-B also has similar directional orientation but the molecules within the planes are arranged into a hexagonal pattern. In smectic-C mesophase, the director is at a small tilt angle with respect to the smectic plane.

3. ***Cholesteric phase*** (also known as chiral nematic) is a mesophase where the nematic state accompanies a progressive twist in the z-direction. The director in each layer is unidirectionally skewed to the layer below it.

The following figure describes the LC phases, graphically (Figure 2-2).

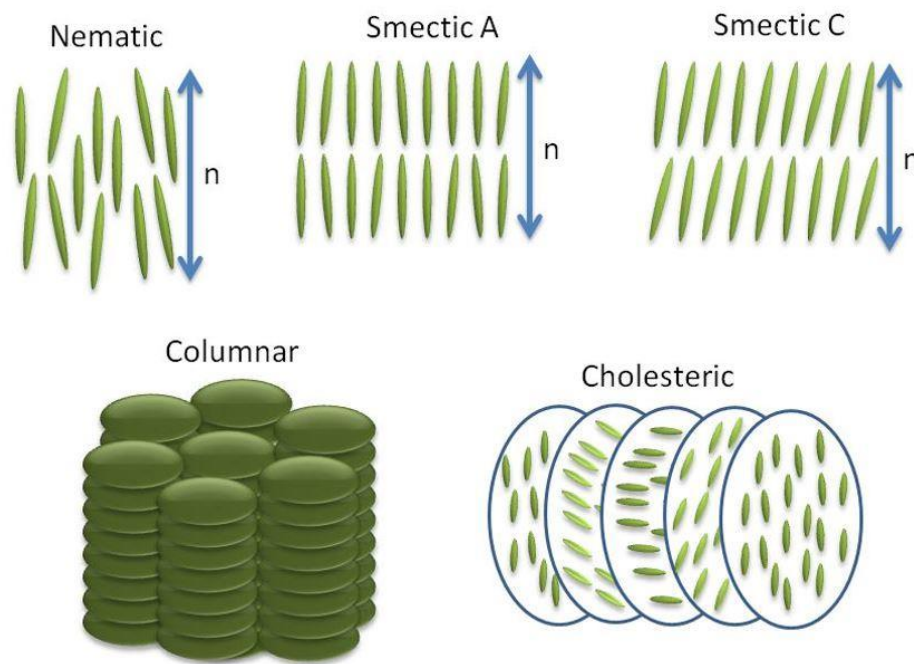


Figure 2-2: Different phases of thermotropic LC systems

Orientational order parameter (s), elastic constant, rotational viscosity and dielectric anisotropy are the most important physical properties of LC material because of the electro-optic characteristics of LC systems strongly depend on these properties.[x] Order parameter is a measure of the degree of order in a system. For rod-like molecules, the

average direction of the long axis of often chosen as the unit vector representing the orientation of the molecule and is defined as,

$$S = \frac{1}{2}(3 \cos^2 \theta - 1)$$

Equation 2-1

Where θ is the angle between the long axis of an individual molecule and the director n . For perfect alignment, $\theta = 0^\circ$ and $S = 1$.

Due to the uniaxial symmetry of the rod-like LC mesogens, the dielectric constant differ in value along the preferred axis (ϵ_{\parallel}) and the perpendicular axis (ϵ_{\perp}). The dielectric anisotropy is defined as,

$$\Delta\epsilon = (\epsilon_{\parallel} - \epsilon_{\perp})$$

Equation 2-1

This anisotropy can be studied using dielectric capacitance and spectroscopic techniques, optical birefringence etc.¹³

2.3 Nanocomposites and Doping with Nanoparticles.

Nanocomposite materials are engineered with two or more constituent materials, one of them being nano-scale sized and with significantly different physical, chemical or electrical properties to obtain the best of all constituent materials. The individual components remain distinct at the nanoscopic scale. The ability to tune the properties of the final structure by altering the concentration of one of the ingredients is a key feature.

Because of the extremely high surface to volume ratio, nanocomposites differ substantially from conventional composites and electrical, optical, thermal and mechanical property may be very different from the starting materials.¹⁴

Doping of LCs with nanoparticle has become a very active area of research. They provide a versatile platform for improving electro-optic, magnetic, plasmonic and physical properties.^{15,16,17} Until now, usage of FNPs like BaTiO₃ has been limited to high permittivity dielectric nanocomposites to increase energy density or power delivery and doping in nematic suspensions to enhance the mesogen ordering, Kerr effect and mild improvement in photoluminescence.^{18,19,20}

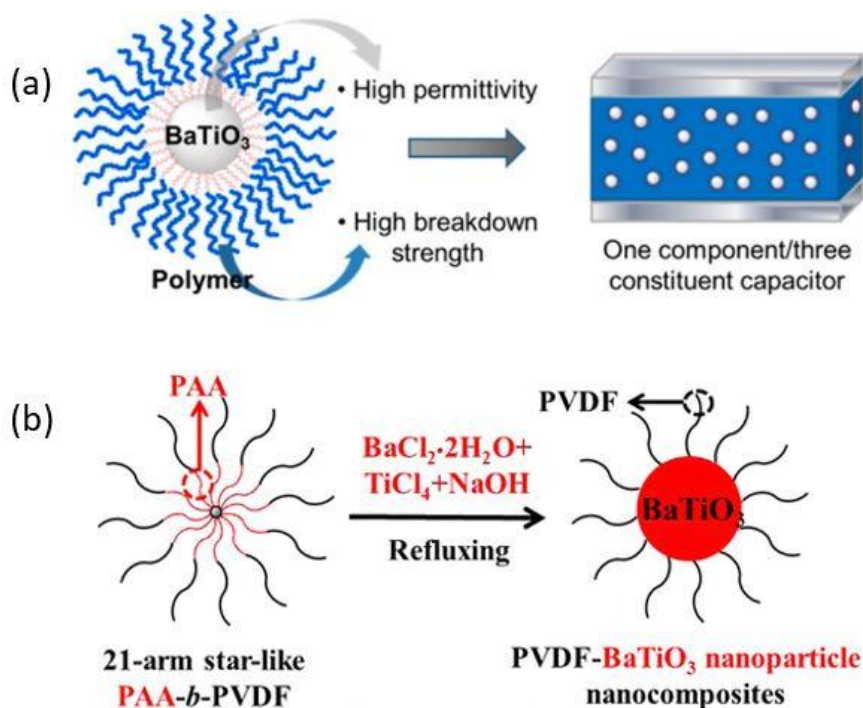


Figure 2-3: (a) and (b) usage of FNPs in high permittivity dielectrics and relaxor materials with enhanced capacitance [Ref 16, 17].

2.4 Motivation and Hypotheses.

Here, we hypothesize and prove that polymer functionalization of FNPs lead to not only enhanced ordering in LCs even in isotropic conditions, but also possible non-volatile memory application. The surface of these FNPs are amenable for functionalization by various amphiphilic and ferroelectric polymers and the resulting hybrid structure exhibits improvement in threshold voltage and mechanical stability.^{19,21}

The use of Liquid crystals (LCs), a well-known display material, for electronic data storage has attracted interest in both fundamental and applied research communities.^{22,23,24} Nanocomposites containing inorganic nanoparticles (NPs) and LC matrices bear a great potential for this application and beyond. The synergistic interactions between NPs and LCs gives rise to new or advanced properties of the hybrid system.

Mobility and order are two key properties for any self-organizing system. LCs possess fluidity, long-range order and by nature they are anisotropic and respond to external stimuli like electric and magnetic fields. As a result of these characteristics, they are considered as an excellent platform for guiding the organization of inorganic NPs into 2D or 3D hierarchical structures with rich optical properties.^{6,25,8, 26} LCs enable dynamic assembly of NPs in two ways: i) they provide structured but flexible medium, and ii) they provide tangential anchoring at the interface of NPs and LCs to stabilize the ordered structures. Hexagonal or Blue phases of LCs, owing to their periodic defects, can induce photon modulation and most importantly, play a pivotal role in 2D long range ordering and self-assembly of 3D hierarchical superstructures.^{27,28,29} Tuneable metamaterial-like application has been shown using such nanocomposites.^{17,30,31}

The presence of plasmonic NPs enhances optical properties of LCs composites without distorting the global nematic director.^{32,33,34} The effect changes when NPs with inherent dipole moment like Barium Titanate (BaTiO₃) ferroelectric NPs (FNPs) are used in place of plasmonic NPs.^{35,16} Several studies have been carried out to understand the

electro-optical and dielectric behavior of LCs when doped with FNPs.^{36,16,37} It is reported that doping of FNPs reduces the switching voltage while enhancing the photoluminescence intensity of the FNP and LC nanocomposite.^{38,39,40} The short range forces between these particles collectively affect dielectric anisotropy, reduce splay elastic constant and decrease response time.^{15,40,41} Pure polymers and hydrocarbons when doped in LCs, have shown similar electro-optic effects.⁴² When polymers are attached on the surface of FNPs like BaTiO₃, they exhibit a huge increase in dielectric strength.^{43,44} Thus, one can hypothesize that a nanocomposite comprising LCs, FNPs and polymers will have very different properties.

Creating programmable memory devices holds great promise in multi-level data storage systems.^{45,46} LC molecules have inherent dipole moment and respond to electric fields by aligning along the direction of the applied field. The field-oriented LC inside a cell with alignment layers, however, reverts back to original orientation once the field is removed. Therefore, such an effect is volatile. Non-volatile memory effects in ferroelectric LCs have been demonstrated by doping carbon nanotubes, both bare and polymer capped gold nanoparticles (Au NPs) and low-frequency dielectric spectroscopy has been a major tool to probe such phenomena.^{47,48} These phenomena have been attributed to ion transfer between LCs to Au NPs and simultaneous ion trapping by polymer corona on the surface of these NPs.⁴⁹ Nematic LCs confined in nano and micro-scale porosities are found to exhibit memory effects due to the field induced anchoring of nematics at the interface of

the pores. This effect has been attributed to the presence of topological defect lines.⁵⁰ In the nematic phase of these nanocomposites, the global director trumps individual molecular orientation and the effect of FNPs on the molecular orientation is hard to distinguish. However, non-volatile memory effect has been reported in the isotropic phase of nanocomposites made of 5CB (4-cyano-4'-pentylbiphenylcarbonitrile) LC and FNPs BaTiO₃.¹⁰ Although these electrically bi-stable, non-volatile memory effects have been reported, practical realization and discreet quantification at the smaller length scale is still challenging.

2.5 Materials and characterization methods

2.5.1 Materials

The nematic 5CB LC was purchased from Sigma Aldrich. The LC has a nematic to isotropic transition (NI) T_{NI} of 35°C. BaTiO₃ FNPs with a diameter of 50±5 nm were purchased from U.S. Research Nanomaterials INC and they were found to be in single phase. Block copolymer (BCP) of polyethylene oxide-b-polystyrene (PEO₄₅-b-PS₆₇₀-SH) containing a small polyethylene oxide block (45 repeating units) and a long polystyrene (670 repeating units) terminated with a thiol functional group was synthesized following the reversible addition-fragmentation chain transfer (RAFT) polymerization procedure as described in the previous report.⁵¹ Another type of BCPs of polystyrene-b-poly(acrylic acid) (PS-b-PAA) with varied polystyrene block length was also produced using the same synthetic approach. Figure 1e depicts what happens when FNPs are introduced into 5CB,

BaTiO₃ molecules carry inherent polarization and as a result, 5CB molecules orient themselves along the dipole field near the interface. A small arrow represents the direction of polarization.

2.5.2 Surface Functionalization and Nanocomposite Preparation

Surface modification of BaTiO₃ FNPs was performed in several stages. First, 2.5 mg BaTiO₃ powder was dispersed in N,N-Dimethylformamide (DMF) and sonicated for 3 hrs. Sonicated solution was centrifuged at 6000 rpm for 20 mins to collect the FNPs and washed with tetrahydrofuran (THF) for three cycles. Finally, the FNPs were redispersed in 5 mL of THF. This control sample was used for measuring the soft-memory effect arising from pristine, non-functionalized FNPs. To attach the polymer ligands, 2.5 g of amphiphilic PEO₄₅-b-PS₆₇₀-SH BCP was dissolved in 5 mL of THF and it was mixed with 5mL premade THF solution containing non-functionalized BaTiO₃ FNPs. The mixture was sonicated for 30 minutes and left undisturbed for 1 hr to promote attachment of the ligands on FNPs surface. The result is a homogeneous colloidal solution containing BaTiO₃ FNPs with BCPs tethered to their surface. Block copolymer chains attach to the FNPs surface via intermolecular interaction and/or van der Waals forces. Since THF readily dissolves 5CB, the pure and polymer modified BaTiO₃ were mixed with 5CB in different vials respectively and sonicated for 1hr to allow homogeneous amalgamation, followed by slow thermal annealing overnight to evaporate THF. The final product was degassed to remove any residual organic solvent and sonicated again for an hour.

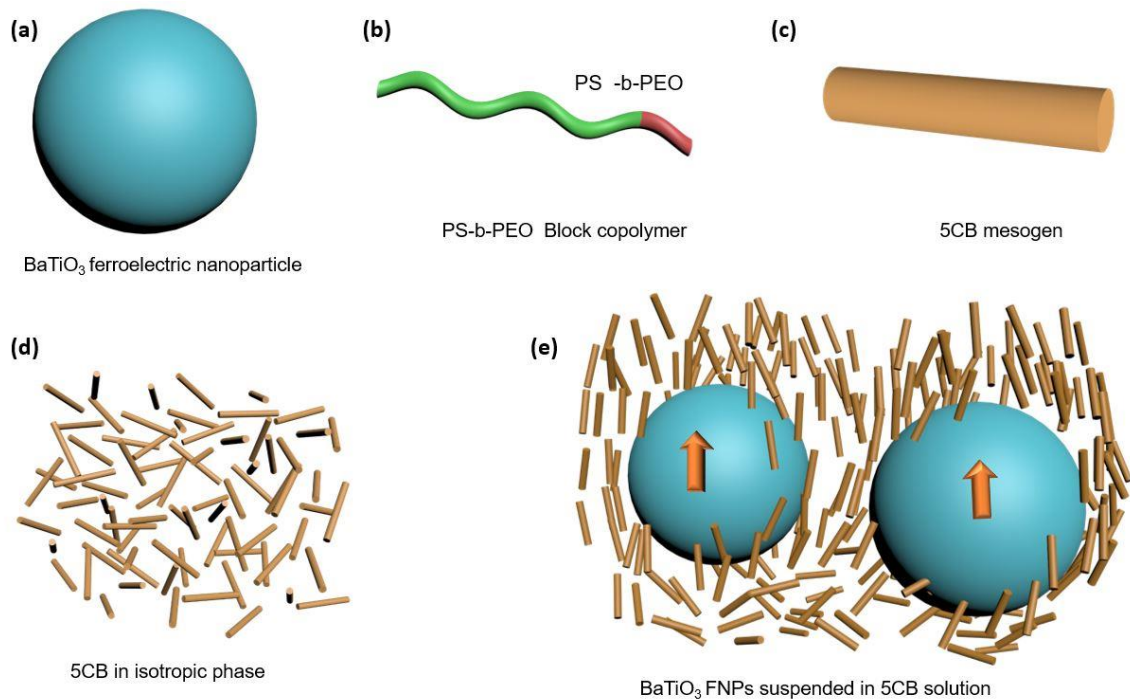


Figure 2-4: Graphical representation of the following materials (a) Barium titanate FNP, (b) Amphiphilic block copolymer, (c) 5CB rod-like molecule, (d) 5CB molecules randomly arranged in isotropic phase, (e) BaTiO₃ suspended in isotropic phase of 5CB showing alignment along the particle interface.

The concentration of BaTiO₃ in weight percentage (wt%) for all cases was chosen such that uniform dispersion was maintained without large aggregates and the global nematic director field wasn't perturbed significantly. Finally, three concentrations were chosen for investigation i.e., $c_1=0.175$ wt%, $c_2=0.275$ wt%, $c_3=0.375$ wt%. Because of the presence of the permanent dipole moment within the molecules, BaTiO₃ FNPs tend to cluster together and above 0.4 wt%, the cluster size becomes large enough to short the LC

cell, affecting the dielectric measurements. Therefore, the reported concentrations for this experiment are below 0.4 wt%.

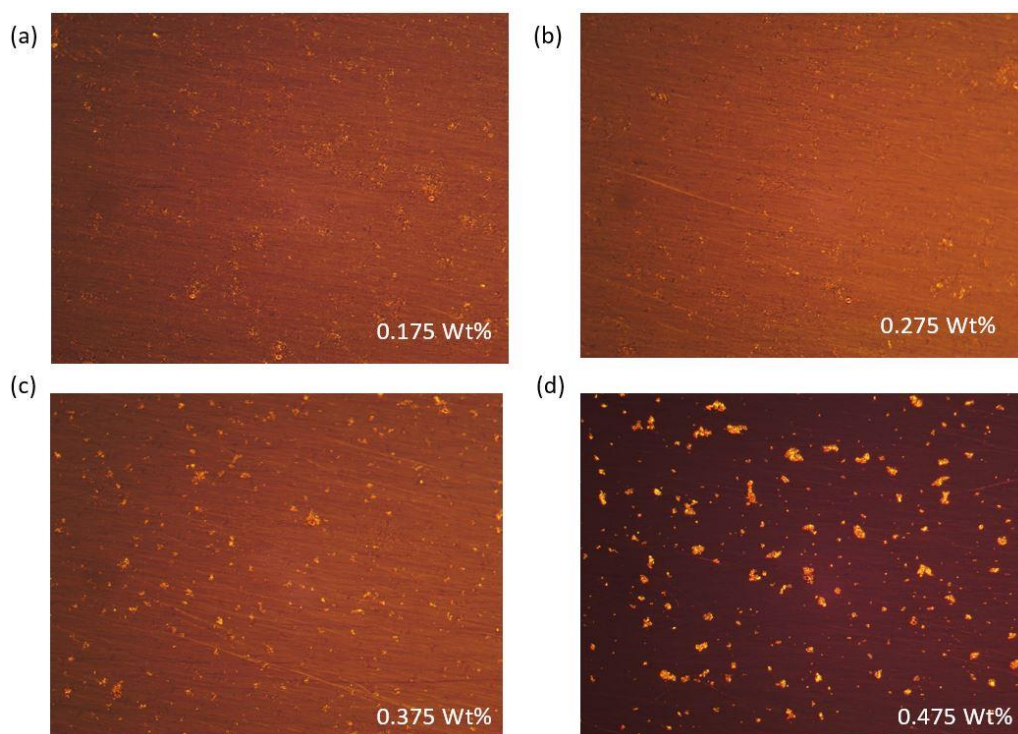


Figure 2-5: Polarized optical microscopy images of BaTiO₃ FNP doped 5CB under cross-polarizers. (a) and (b) show minimal texture, while (c) has very minimal aggregates but (d) has large aggregates that could short the cell.

2.5.3 Dielectric Characterization

Dielectric measurements were carried out using a custom apparatus setup consisting of microscope thermal stage, a programmable precision temperature controller, waveform generator- amplifier and automatic liquid crystal tester (ALCT), all manufactured by Instec, Inc. Commercially available LC cells (SA100A200uG180, planar rubbed) with 1

cm² semi-transparent indium tin oxide electrode area, 1° pretilt angle and a spacing $d = 20$ μm was used for our experiments. Design of the custom I-V setup is made up of a Stanford Research Systems SG394-4 signal generator and a lock-in amplifier that controls the voltage (V) and current input (I). These two apparatus were controlled virtually by a computer that is configured to LabVIEW interface and all the readings were recorded in this way for further processing. The voltage was set to vary from 0 V to 30 V in a cyclical fashion for finite number of cycles and in an incremental step of 0.1V at 1 KHz frequency. An AC field would deter any remnant ions in the 5CB from accumulating at the electrode interface and thereby shorting the circuit.

Dielectric characterization experiments were conducted in the Soft Matter and Nanomaterials Lab at the United States Naval Academy. Scanning Electron Microscopy (SEM) was done using Hitachi SU-70 field emission scope at the Advanced Imaging and Microscopy (AIM) laboratory at the University of Maryland.

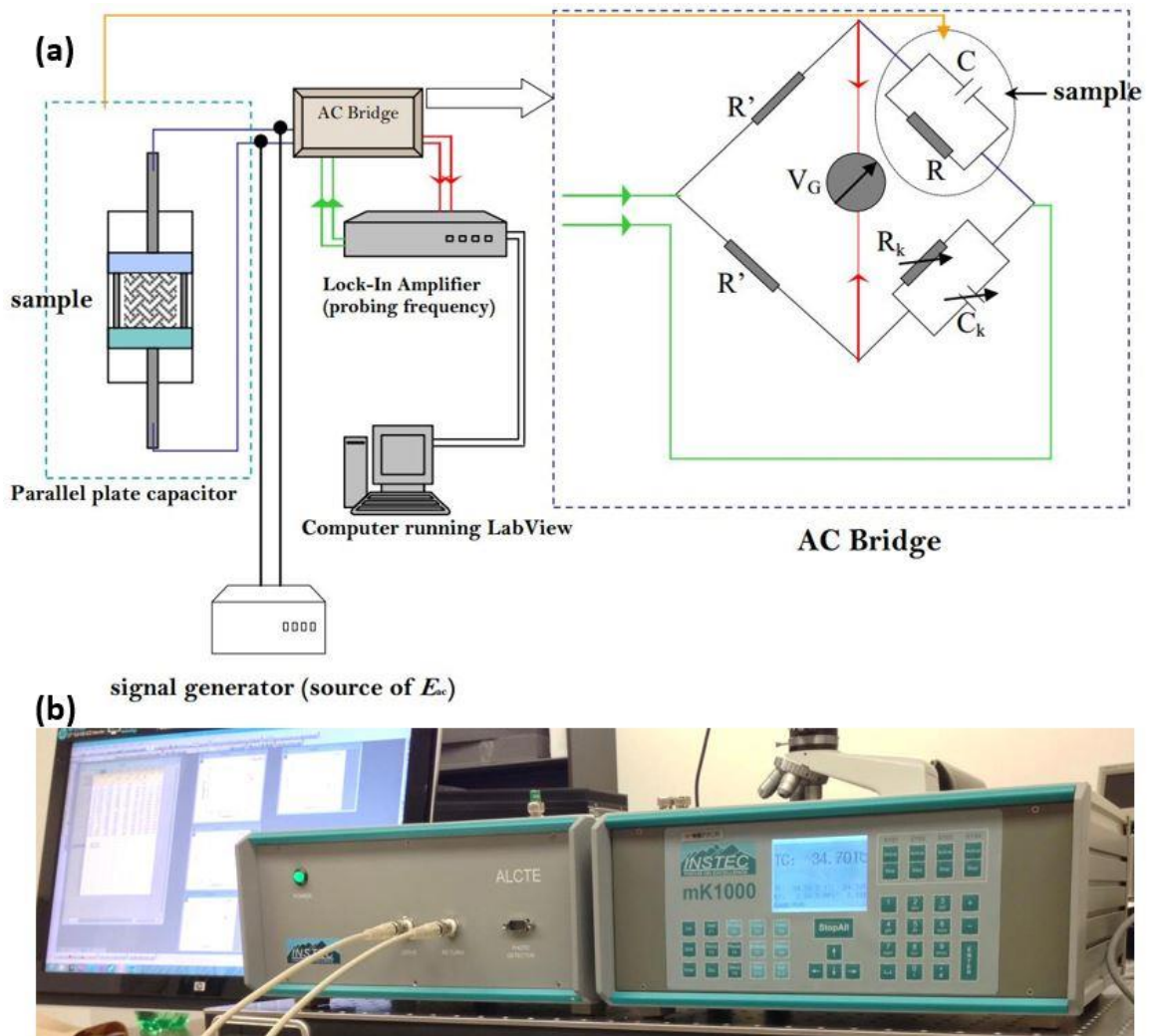


Figure 2-6: (a) schematic of the circuitry of the dielectric measurement setup at USNA. (b) Automatic liquid crystal tester (ALCTE) equipment connected to a programmable precision stage and LabVIEW interface. (Courtesy: Dr. Raj Basu, US Naval Academy).

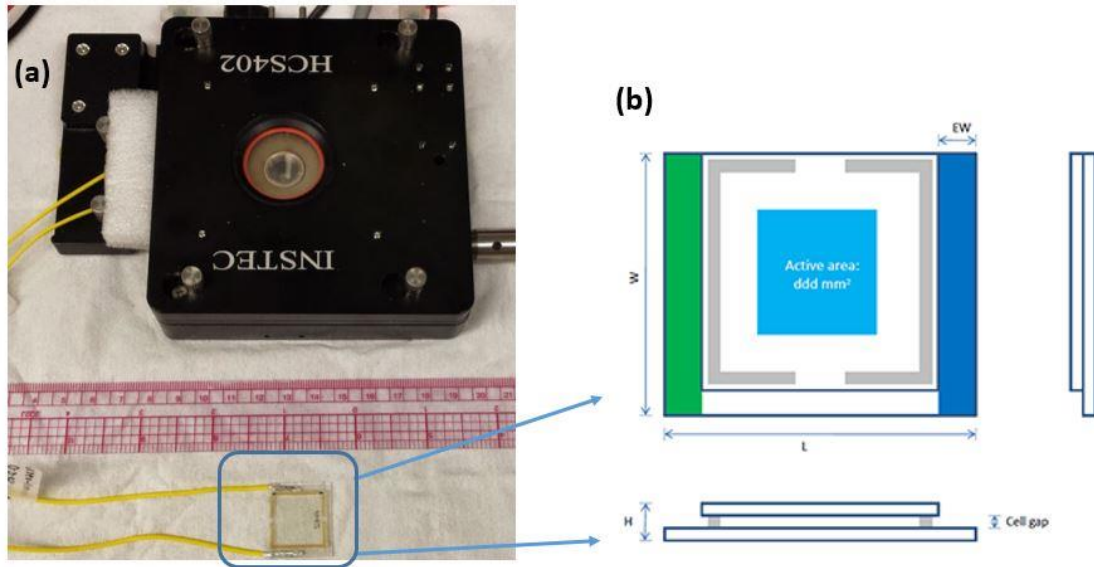


Figure 2-7: (a) programmable microscope hot and cold stage with LC cell. (b) Schematic of the LC cells coated with ITO from Instec Inc.

2.6 Experimental Findings and Discussions.

Here, we report a giant electromechanical soft-memory effect found in a nanocomposite system comprised of isotropic phase of an LC doped with block BCP modified FNPs. The soft-memory effect we are referring to in this report is a *non-volatile electromechanical effect* at the interface of LC molecules and FNPs surface. As shown in Figure 2-7, the automatic liquid crystal tester was fully customized and automated with a computer interface.

The synergistic effects of polymer ligands and FNPs lead to the formation of several nanoscopic domains of local paranematic ordering, having different anisotropy than the

global nematic phase. The size of such ordered domains is much larger than the domains found in nanocomposites of bare BaTiO₃ FNPs in 5CB. The combined effect of BCP-modified FNPs in the LC, as studied by the dielectric hysteresis effect, is significantly larger than the sum of individual contributing components i.e., pure polymers and pristine BaTiO₃ FNPs.

We chose one of the most widely used systems, 5CB for LCs and BaTiO₃ for FNPs. The topology of these polymer-modified FNPs can be affected by the external stimuli and hence, both kinetics and thermodynamic pathway play a role in alignment of mesogens around these particles.

The 5CB LC is dielectrically anisotropic in nature and possesses long-range order. Its global nematic director (\hat{n}) is defined as the average molecular direction of preferred orientation of individual molecules. As a result of this anisotropy, it has two different dielectric constant components i.e., dielectric constant along the global nematic director, ϵ_{\parallel} and dielectric constant in the orthogonal direction, ϵ_{\perp} , as shown in Equation 1. In a parallel-plate planar cell, the rubbing direction promotes homogeneous alignment of the LC director. In the nematic phase, the LC exhibits Fréedericksz transition behavior, where an electric field (E) is applied across the cell and the nematic director orients from a planar configuration (ϵ_{\perp}) to a homeotropic configuration (ϵ_{\parallel}). This director reorientation occurs because the LC experiences a rotational torque proportional to $\Delta\epsilon E^2$ in the presence of the

electric field. When the field is switched off, the director reorients back to planar configuration due to the LC's long range splay elastic interaction and the surface anchoring mechanism in the cell. When the temperature is raised above T_{NI} , the global nematic order is destroyed and the Fréedericksz transition is no longer observed.⁵²

Figure 2-8 shows the dielectric constant as a function of electric field in nematic phase for pure 5CB, 5CB doped with bare BaTiO_3 (5CB/ BaTiO_3) and 5CB doped with polymer functionalized BaTiO_3 (5CB/BCP-modified- BaTiO_3), at a doping concentration of 0.275 wt% of FNPs. As the applied field across the cells was raised, the dielectric constant increased, showing a typical Fréedericksz transition with a threshold field of $0.04 \text{ V}/\mu\text{m}^{-1}$ for all three samples. No hysteresis effect in the dielectric constant was observed on turning the field down to zero in the nematic phase. The nematic phase shows dielectric anisotropy as indicated by Equation 2-2. For a positive dielectric anisotropic LC, $\epsilon_{\parallel} > \epsilon_{\perp}$, and so, the director field reorients parallel to an applied electric field. In a uniform homogeneously aligned parallel-plate cell configuration, the nematic director is aligned perpendicular to the applied electric field due to surface anchoring but the director can reorient parallel to the field if the field magnitude is above some critical threshold. This is the essence of a Fréedericksz transition.

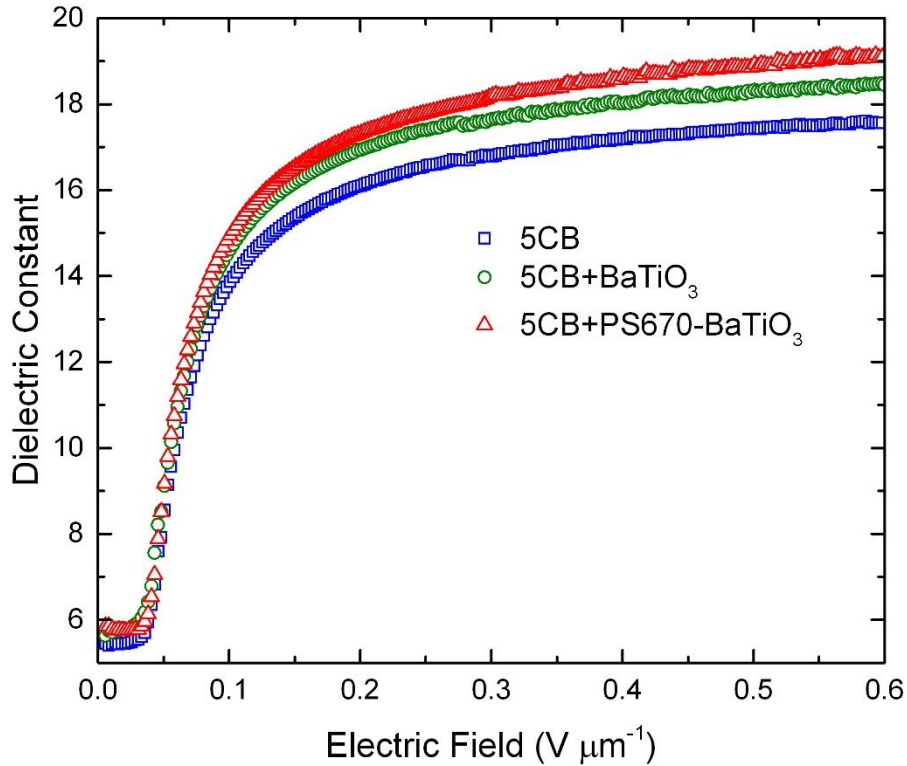


Figure 2-8: Dielectric constant of pure 5CB, 5CB doped with BaTiO₃ FNPs and polymer modified BaTiO₃ FNPs at 0.275 wt %. Dielectric constant is plotted against applied RMS field ($f=1$ KHz) and in nematic phase of LCs (25°C).

BaTiO₃ FNPs carry a spontaneous polarization $P = 0.26 \text{ C}\cdot\text{m}^2$.⁵³ As a result they enable very strong local electric fields on the order of $10^{10} \text{ V}\cdot\text{m}^{-1}$ near the surface. This local field, E_{FNP} attenuates as $1/r^3$. The presence of E_{FNP} creates nanoscopic domains where LC mesogens orient along E_{FNP} surrounding the FNPs, and we call these regions — *pseudonematic domains*. In the nematic phase, these short-range domains align with the global nematic director to reduce the free energy of the nematic matrix. These domains

collectively increase the nematic orientational order, increasing the dielectric anisotropy in the nematic phase of the system, as shown in Figure 2-9.

The dipole moment magnitude for a 5CB molecule is $p = 6.5 \text{ D} = 2.15 \times 10^{-29} \text{ C}\cdot\text{m}$. When the LC molecule aligns with E_{FNP} close to the FNP, the associated energy can be written as $U_{\text{FNP}} = -\vec{p} \cdot \vec{E}_{\text{FNP}} \sim -10^{-19} \text{ J}$.⁵⁴ The thermal energy in the isotropic phase of 5CB at $T = 42^\circ\text{C} = 315 \text{ K}$ is $U_{\text{thermal}} \sim k_{\text{B}}T \sim 10^{-21} \text{ J}$. Apparently, the thermal energy is too small to eliminate the FNP-induced LC-order in the isotropic phase. Due to the presence of these domains, the isotropic phase of 5CB/BaTiO₃ nanocomposite maintains a net dielectric anisotropy and is expected to interact with the external electric field.

Figure 2-9 shows the dielectric constant as a function of applied field in the isotropic phase ($T = 42^\circ\text{C}$) for pure 5CB, 5CB/bare BaTiO₃, and two different 5CB/BCP-modified-BaTiO₃ samples as listed in the legend. Pure 5CB shows a featureless behavior in the isotropic phase as expected. The hybrid systems show an increase in the dielectric constant above a threshold field, exhibiting a Fréedericksz-like transition. The dielectric constant for these nanocomposite systems does not relax back to its original value on turning the field down to zero, manifesting a dielectric hysteresis effect. The hysteresis area correlates to the soft-memory effect in the hybrid samples. The memory effect for the 5CB and pure BaTiO₃ nanocomposite (sample 1) can be seen from the red (□) curve in

Figure 2-9; the dielectric anisotropy holds its value ($\Delta\epsilon_{5CB}^{iso} / FNP = 0.4$) even when the field is switched off.

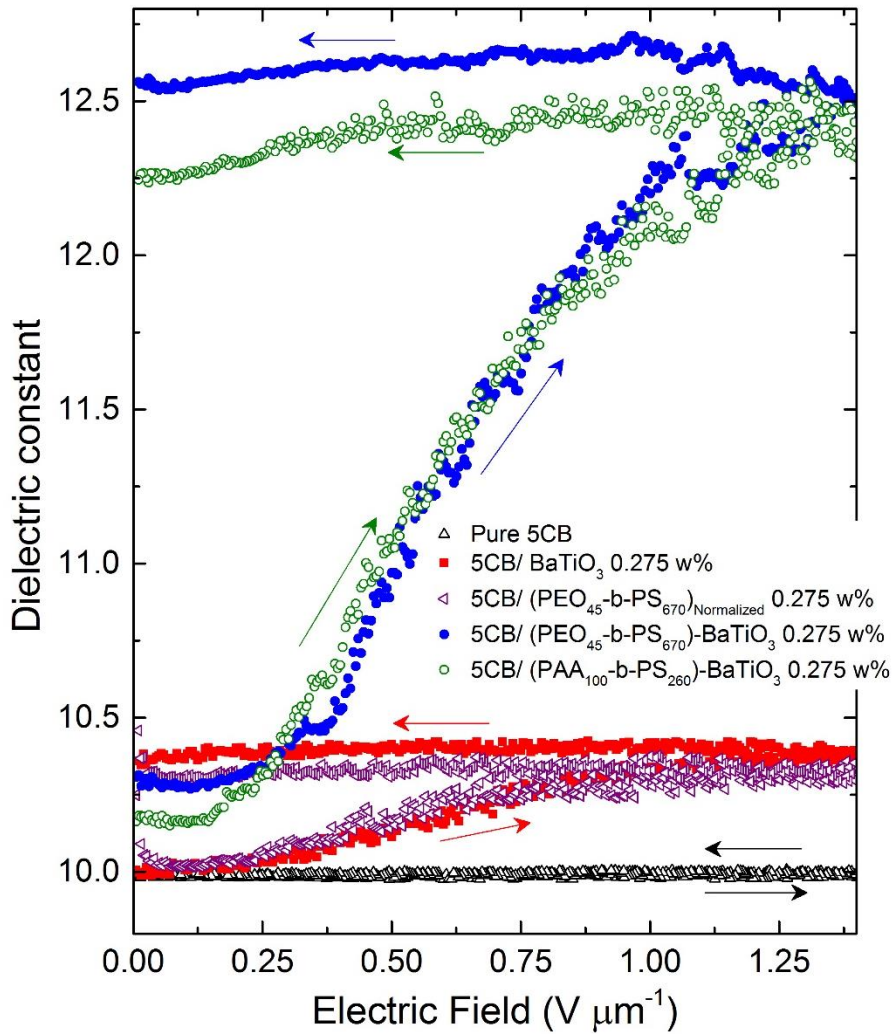


Figure 2-9: Dielectric hysteresis of pure 5CB (black), pure PEO45-b-PS670-SH polymer (purple) doped in 5CB, 5CB/ bare $BaTiO_3$ composite (red), polymer functionalized $BaTiO_3$ FNPs (blue and green) as a function of applied electric field in isotropic phase ($T= 42^\circ C$).

Even though the hybrid system contains short-range pseudonematic domains, the global nematic order is still absent in the isotropic phase. Therefore, there is no long-range elastic interaction present in the isotropic phase. Accordingly, these isolated pseudonematic domains do not interact with the aligning layers of the LC cell. Therefore, when the field is turned off, there is no restoring force to mechanically torque these domains back into original orientation in the isotropic phase and the domains stay oriented, as schematically shown in Figure 2-11. The hysteresis area in the doped hybrid sample can also be directly attributed to the enhanced pseudonematic domains as shown in the Figure 2-10. If we consider a single dimer of bare BaTiO₃ and PEO₄₅-b-PS₆₇₀-SH polymer doped FNP dimer in isotropic 5CB, the polymer chains act as a scaffold for the mesogens to attach to and active area becomes roughly 6 times larger.

In Figure 2-10, the hysteresis curve for sample 2, 5CB/PEO₄₅-b-PS₆₇₀-SH polymer functionalized BaTiO₃ FNPs (blue curve) clearly shows a giant increase in the magnitude of dielectric anisotropy ($\Delta\epsilon_{5CB}^{iso} / (PEO_{45}-b-PS_{670})_{FNP} = 2.4$) and a six-fold increase (ratio of dielectric anisotropy of sample 2 to sample 1 = 6) in the hysteresis area compared to nanocomposite sample containing just 5CB and pure BaTiO₃ FNPs at the same wt% concentration.

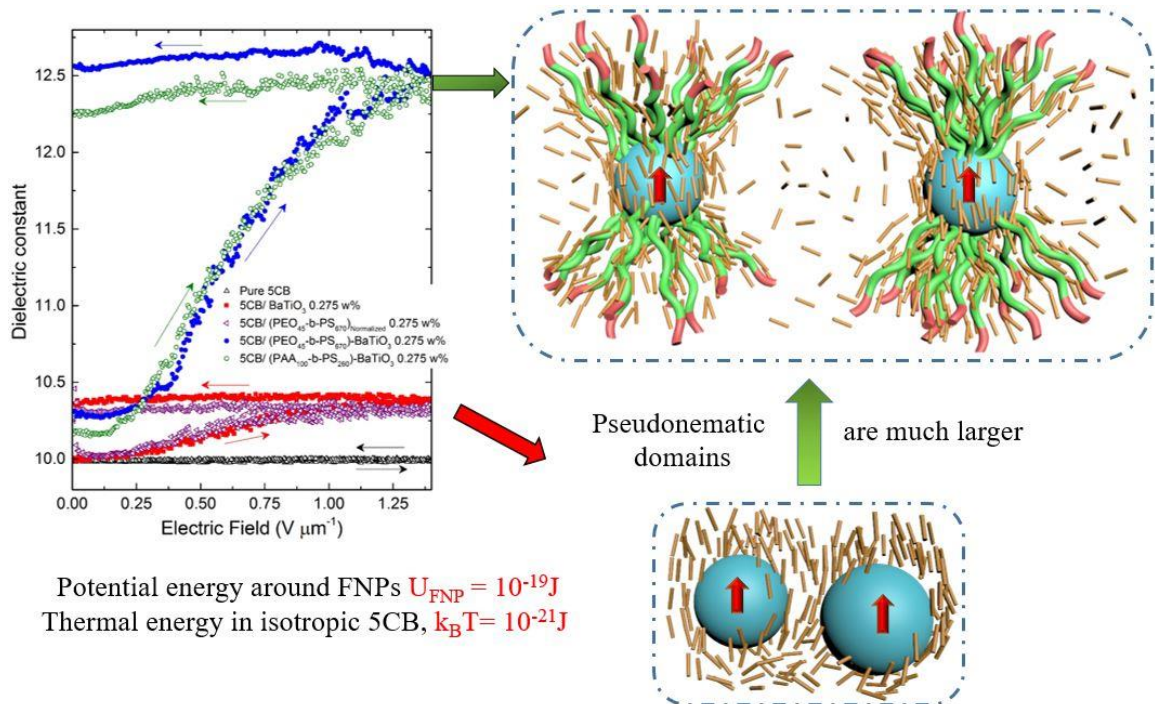


Figure 2-10: Schematic representation of enhanced pseudonematic domains as a result of polymer functionalization of FNPs and the subsequent increase in the dielectric anisotropy.

If we compare this value to the dielectric anisotropy of nematic 5CB, ($\Delta\epsilon_{5\text{CB}}^{nem} = 12$), we can estimate that even in isotropic phase, 20% of all the mesogens have directional orientation compared to fully nematic 5CB. As stated earlier, in both cases, the thermal perturbations ($k_{\text{B}}T$) is not large enough to induce any changes to the order of the mesogens at the interface.

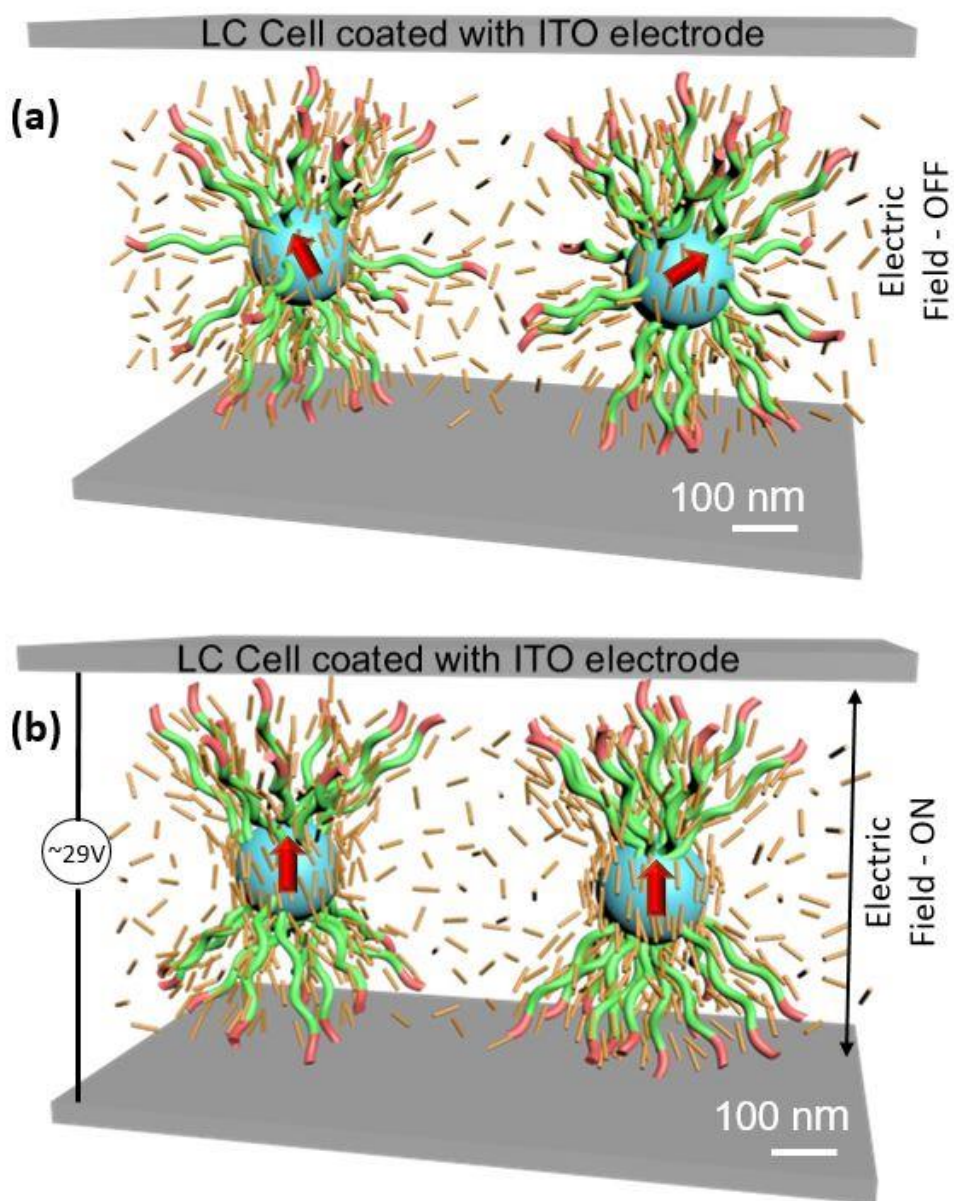


Figure 2-11: (a) When there is no applied field across the LC cell, the mesogens are randomly oriented (b) we see that upon the application of AC field across the LC cell, pseudonematic domains mechanically rotate BaTiO₃ FNPs in the direction of the field. The density of mesogens is greater along the poles. This remnant polarization leads to giant soft-memory.

An electric field of $1.3 \text{ V}/\mu\text{m}^{-1}$ was first applied to a hybrid system for 30 seconds to initiate the reorientation of pseudonematic domains and then switched off. The dielectric constant was monitored using a capacitance bridge as a function of time for the next 72 hours and plotted in the Figure 2-12. No significant change was observed in this time period.

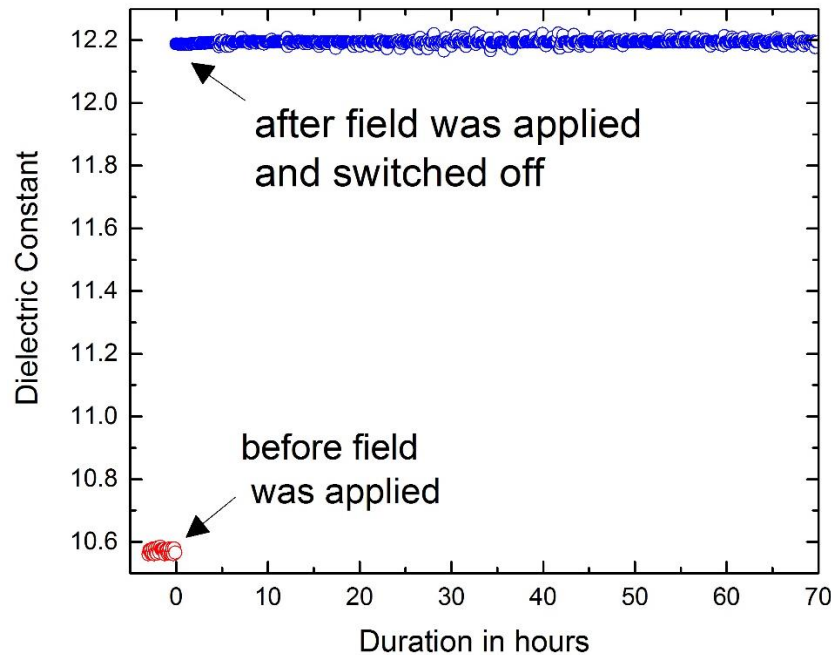


Figure 2-12: Non-volatility of pseudonematic domains in the isotropic phase of 5CB. The dielectric constant maintains a constant value over a period of 3 days.

This is the essence of a non-volatile nano-electromechanical memory effect, as the electric field *mechanically* rotates the domains at the nanoscale. In addition, the absence of the back flow in the thin LC cell also allows the domains to stay oriented. The thermal

diffusion mechanism in this case takes days to randomize the domains in the cell, as can be seen from the Figure 2-12.

The limiting factor in doping LCs with NPs is the severe aggregation of NPs in LCs. Several studies have been carried out on attaching a variety of polymer and mesogenic ligands onto the surface of inorganic NPs to enhance their stability in the LC matrix and induce memory effect. We doped 5CB with FNPs functionalized with a BCP of PS-b-PAA. The PAA block is expected to bind strongly with BaTiO₃ FNPs surface via a combination of chemical and van der Waals interaction.⁵⁵ Even with shorter PS chain in the PS-b-PAA BCP, we noticed it produced comparable hysteresis effect as the PEO₄₅-b-PS₆₇₀-SH polymer (See Figure 2). This can be explained by the stronger binding of PS-b-PAA to BaTiO₃ than PEO-b-PS-SH BCP, because of the multiple binding sites on PAA block. Our measurements were limited by the availability of polymer that had longer PS block and higher affinity PAA block.

To understand the roles of these factors on this soft-memory, especially the role of polymer chemistry and FNPs concentration, we have studied three different concentrations of 5CB / PEO₄₅-b-PS₆₇₀-SH modified BaTiO₃: 0.175 wt%, 0.275 wt% and 0.375 wt%. Figure 2-14 shows the effect of the dopant concentration on the hysteresis effect. To further understand this huge increase in dielectric hysteresis in detail, we studied (i) the effect of only pure PEO₄₅-b-PS₆₇₀-SH in 5CB, and (ii) the dispersibility of BaTiO₃ when functionalized with PEO₄₅-b-PS₆₇₀-SH.

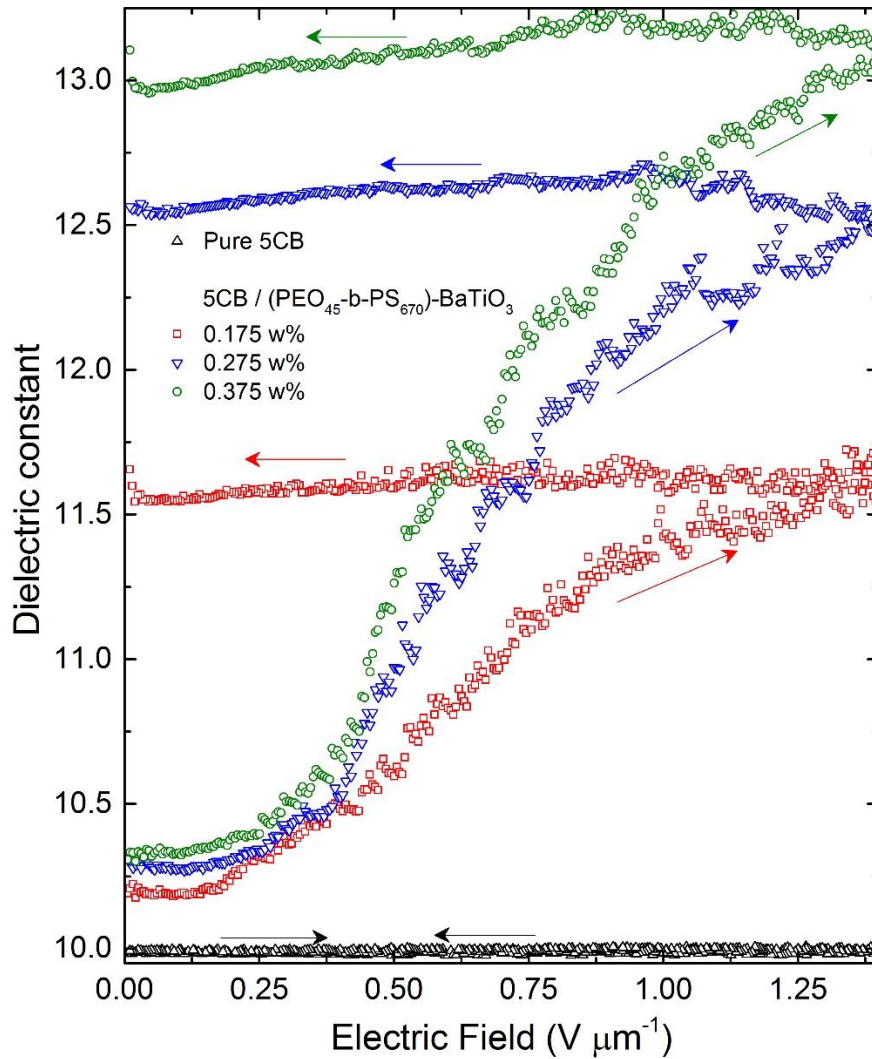


Figure 2-13: Dielectric hysteresis area of PEO45-b-PS670-SH polymer functionalized BaTiO₃ nanocomposite as a function of concentration of dopants. Inset shows the dielectric hysteresis for various polymers that were used to functionalize BaTiO₃ and dope 5CB LC.

The repeating units of hydrophobic PS block of BCPs have electron-rich benzene ring that can interact with biphenyl group of 5CB via π - π stacking interaction. Therefore,

a polymer that has more units of hydrophobic PS block, will favour aligning with 5CB molecules because of this π - π stacking. While pure 5CB does not produce any hysteresis, increasing the dopant concentration results in larger dielectric hysteresis owing to more pseudonematic domains. Homopolymer of PAA₆₀₀ alone (without the PS block) cannot produce the same effect as PS-b-PAA which contains PS block, due to absence of π - π stacking interaction (red curve, Figure 2-9). However, an introduction of even small PS block (PS₂₆₀) with PAA₁₀₀ can produce much larger dielectric hysteresis (green curve, Figure 2-9).

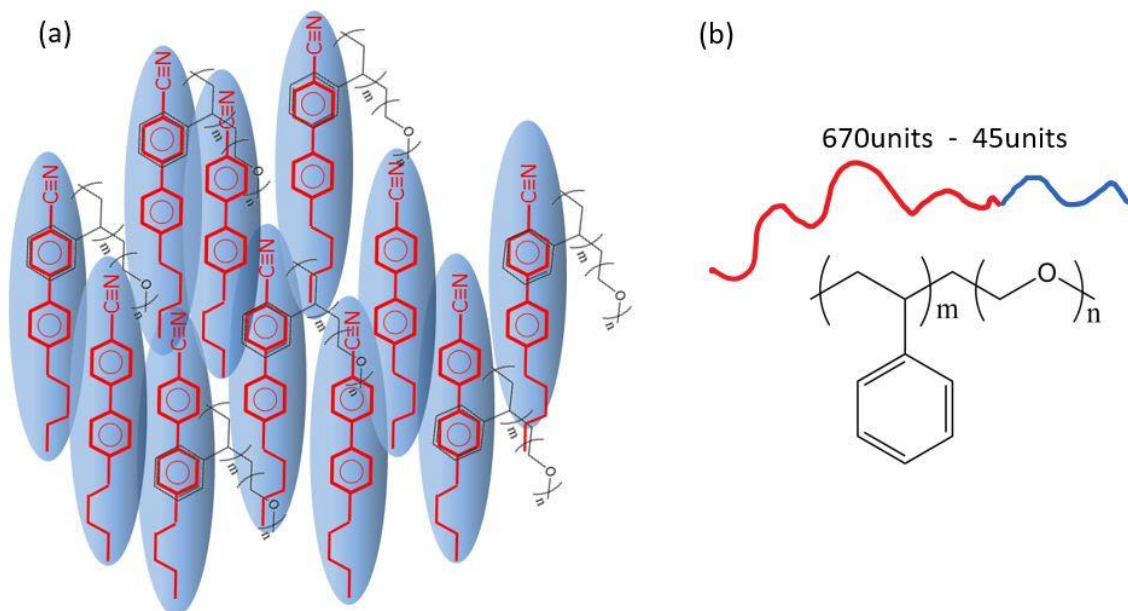


Figure 2-14: (a) Molecular structure of PEO45-b-PS670-SH BCP. (b) Schematic illustrating the π - π stacking interaction between 5CB mesogens and benzene rings of polystyrene units.

The end-to-end length of each hydrophobic PS₆₇₀ block in a polymer chain is calculated to be around 6-7 nm. Increasing the thickness of polymer brushes, depending on the conformation, leads to several structural modifications. First, rotational viscosity of the LC mesogens around the FNPs changes as a result of new anchoring onto these BCP chains and the resulting pseudonematic domains are bigger by 10-14nm. Here, the available electromechanical force by which the particles can be rotated also becomes higher. We then doped 5CB with pure PEO₄₅-b-PS₆₇₀-SH such that the wt% of the dopant is approximately equal to the weight of the polymer chains tethered on the BaTiO₃ FNPs surface. This normalized weight was essential as not all polymers we use for

functionalization goes onto the surface of the FNPs. In this case, we also noticed a hysteresis curve (purple) as shown in Figure 2-11. This result clearly suggests that the presence of pure PEO₄₅-b-PS₆₇₀-SH in 5CB also form paranematic domains due to the π - π stacking between the LCs and the polymer chains. These domains also interact with the external electric field, showing a hysteresis effect. However, as clearly seen in Figure 2-10, the hysteresis effect of 5CB / PEO₄₅-b-PS₆₇₀-SH polymer functionalized BaTiO₃ is significantly larger than the sum of individual contributing components i.e., the pure polymer and the pure BaTiO₃ FNPs.

Due to the dipole-dipole interaction between the FNPs, it is expected that some FNPs are present in aggregates in a solution, resulting in antiparallel-dipole arrangements. An antiparallel-dipole configuration can be approximately treated as a quadrupole, whose field magnitude drops as $\sim 1/r^4$ and hence the pseudonematic domains formed by the FNP-clusters would have smaller anisotropy. On the other hand, the presence of the polymer ligands on the FNP surface prevents the aggregation of FNPs to a large scale. To visually examine the effects of polymer ligands on aggregation and dispersability, we prepared two samples: i) 5CB and bare BaTiO₃ FNPs and ii) 5CB and BaTiO₃ FNPs functionalized with PEO₄₅-b-PS₆₇₀-SH polymer. After preparation, they were allowed to stabilize for 10 hours and then a drop of each of sample in THF solution was deposited on a silicon substrate for Scanning Electron Microscopy (SEM) imaging (the substrate was washed by acetone, ethanol, and isopropanol to remove any organic impurities). Figure 2-15 shows

representative SEM images of these samples. It was apparent that bare 50 nm BaTiO₃ sample formed several micron-sized aggregates (Figure 2-15 a & c), whereas PEO₄₅-b-PS₆₇₀-SH polymer functionalized BaTiO₃ FNPs showed a much better dispersion (Figure 2-15 b & d).

Without large clusters, therefore, the polymer functionalized BaTiO₃ FNPs retain their strong dipolar electric field that drops as $\sim 1/r^3$ and create pseudonematic domains with a higher dielectric anisotropy and a larger size, as illustrated in the schematic in Figure 2-10. Due to this enhancement in the pseudonematic domains, the polymer-functionalized-BaTiO₃ samples exhibit a giant hysteresis effect. It is reported that the size of the inorganic NP's, the nature of the capping ligand, the concentration of the dopant, the length of polymer chain, all play a major role in affecting the dispersibility, long-range ordering and electro-optic properties.^{9,14,20, 56}

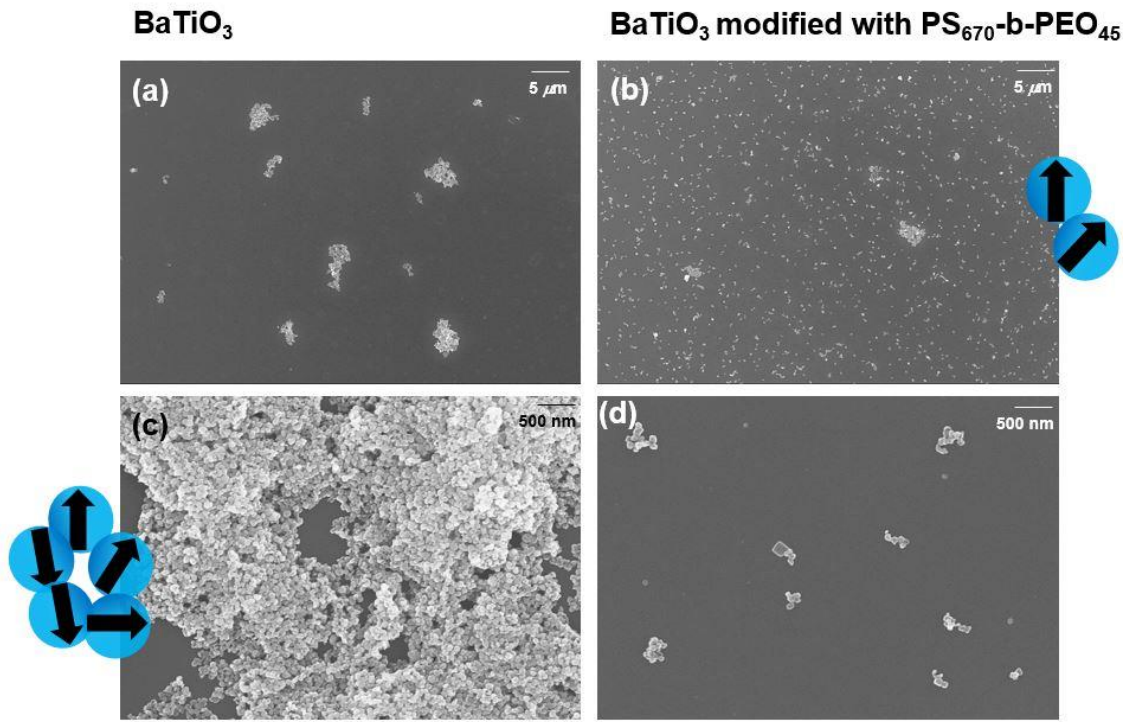
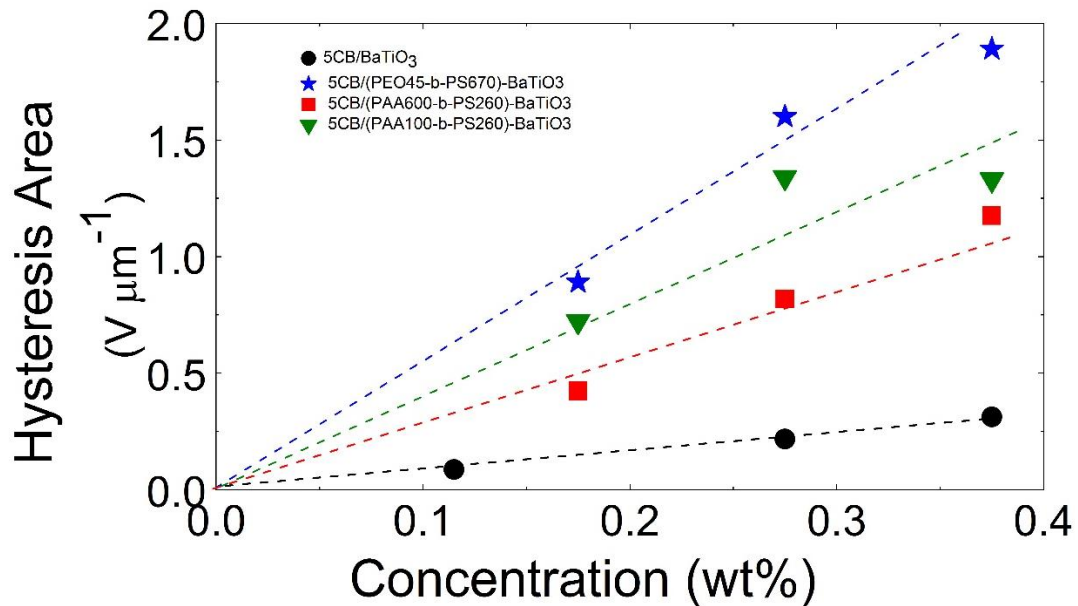


Figure 2-15: Scanning Electron Microscopy images of the pure BaTiO_3 and $\text{PEO}_{45}\text{-b-PS}_{670}\text{-SH}$ BCP functionalized BaTiO_3 FNP's. From the inset (a) and (c), we can infer that clusters and random aggregates are prevalent. Functionalized samples as shown in (b) and (d) provides evidence of uniform colloidal dispersion.

With increasing concentration of the dopant, we see larger dielectric hysteresis, indicating the presence of more number of pseudonematic domains at higher concentrations. The Figure 2-16 explains the role of different polymer chemistry on the dielectric hysteresis area. Finally, polymers not only act as anchoring scaffold for LC mesogens to orient preferentially due to $\pi\text{-}\pi$ stacking interaction, but they also play an

important role in the stabilizing FNPs in the LC matrix, thus dramatically enhancing the soft-memory effect.



In conclusion, we have shown that 5CB doped with BCP functionalized BaTiO₃ FNPs yield giant enhancement of soft-memory effect under isotropic conditions and the memory is non-volatile and stable for several days. Dielectric anisotropy ($\Delta\epsilon$) is enhanced by multi-fold by simple attachment of BCP chains on the surface of NPs. Both polymer chemistry and concentration dependent studies have been conducted to understand the phenomena. Doping LCs with functional NPs is an effective way of enhancing the electrical and optical behaviour of this soft matter system. We expect that the hybrid nanocomposite's $\Delta\epsilon$ can be further enhanced by optimizing the composition or by attaching

ferroelectric polymer attached to a ferroelectric nanoparticle. This new finding provides insight to design a programmable, completely erasable non-volatile memory device.

Chapter 3

Dielectric Spectroscopy of Gold Nanorods

The nematic LC has been the ubiquitous standard for display devices. The flat panel (TFT, OLED, AMOLED etc.) industry has a global revenue of ~ USD \$130 Billion as of 2015 and is expected to rise sharply over the next few years.^{56a} Recently, the industry has been facing some challenges for advanced applications including sourcing precious metals for ITO coating. There has been tremendous interest in the research community to discover alternative material for optical filters and display devices. One such candidate is gold nanorods (AuNRs).⁵⁷ AuNRs offer many advantages as they can be solution processed, offer unique SPR-based anisotropic optical properties. Because individual AuNRs are larger than LC mesogens, the anisotropy of electric susceptibility of AuNRs is large enough (comparable to thermal excitations $\sim k_B T$) to be coupled to electric fields. Because of this reason, AuNRs can be aligned using electric fields and tuned by light and can be assembled into dimers, chains and even bulk metamaterials.^{17,58,59} Unlike LCs which depend on near neighbor interaction for their alignment and a solution of AuNRs can be made into an extremely thin display, continuously tuned and offer the possibility of ultra-fast switching ($< 5 \mu\text{s}$). Until now, there has not been a systematic study of field dependent orientational behavior of AuNRs and dielectric loss at various frequency regimes. We initiated a systematic study to probe these features and the results from the recent experiments have been documented here in this chapter.

3.1 Materials and Characterization Methods

Solution-based synthesis of AuNRs is normally done using CTAB and sodium borohydride (NaBH_4), as CTAB has a non-uniform affinity for the Au sphere's surface due to the lattice structure of the gold. This allows the Au spheres to grow into an anisotropic ellipsoidal shape. To maintain purity and minimize polydispersity within samples, we opted to purchase high-purity AuNRs from Nanopartz™ Inc. We chose AuNRs of three different aspect ratios and the details are tabulated in the Figure below. Thiol terminated polystyrene polymer (P4434-SSH) with a molecular weight of 50,000 (Mn) was purchased from Polymer Source Inc. and used as is. Tetrahydrofuran (THF), refractive index matched oil and toluene were purchased from Sigma Aldrich.

The solution synthesis of AuNRs using CTAB makes them dispersible in polar solvents but makes running any dielectric measurements impossible. For this reason, it is important to disperse the nanorods in a non-polar solvent and be able to torque them with electric fields. The solvent should support long range orientation of AuNRs and provide minimal torqueing resistance.

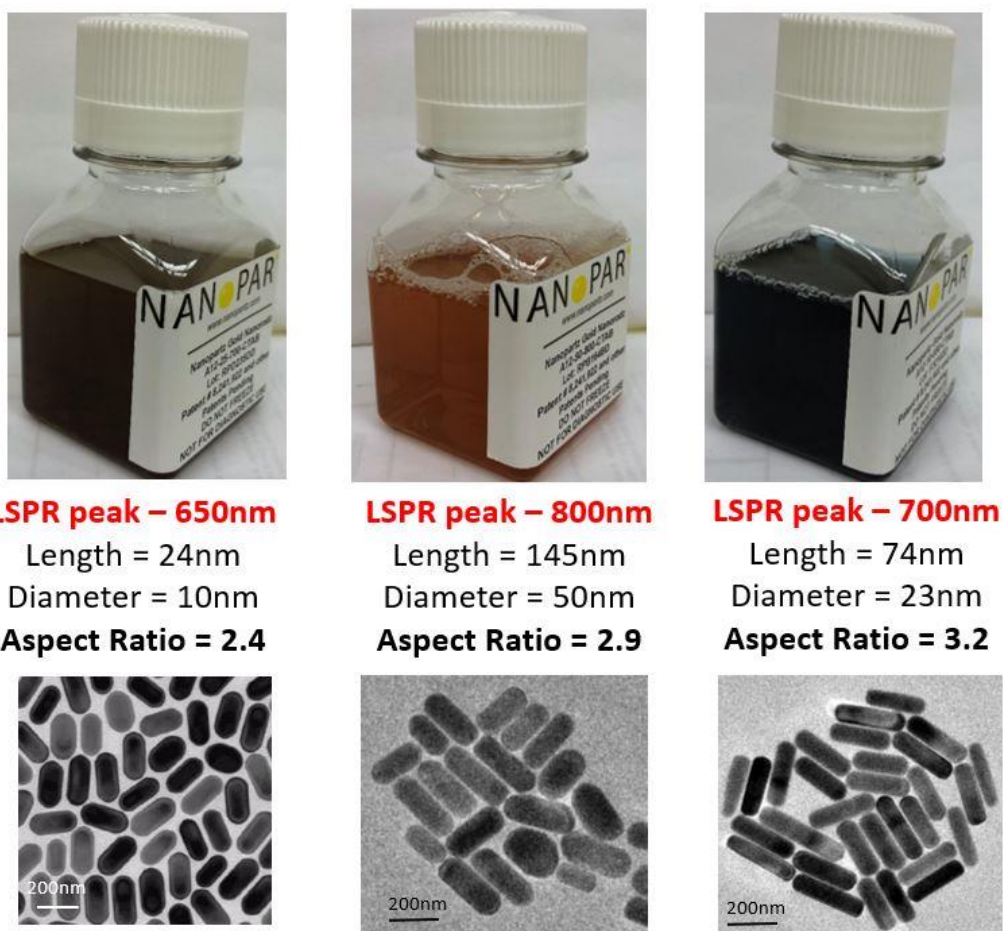


Figure 3-1: AuNRs with their respective LSPR peak and transmission electron microscopy (TEM) images.

So, coating the AuNRs with polymer ligands and then phase transferring into organic solvents was accomplished as detailed below and the images show the sequence of steps involved.

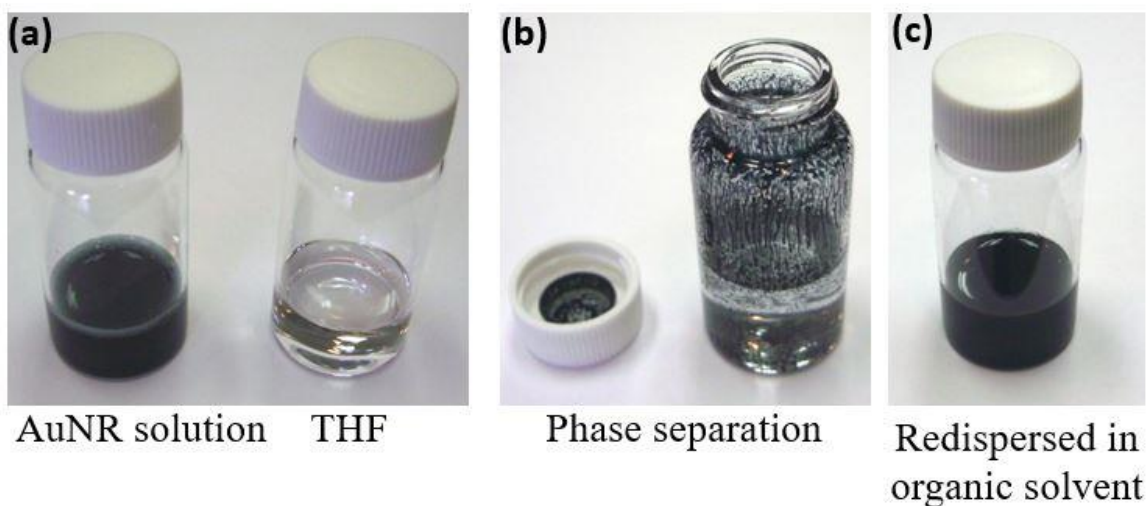
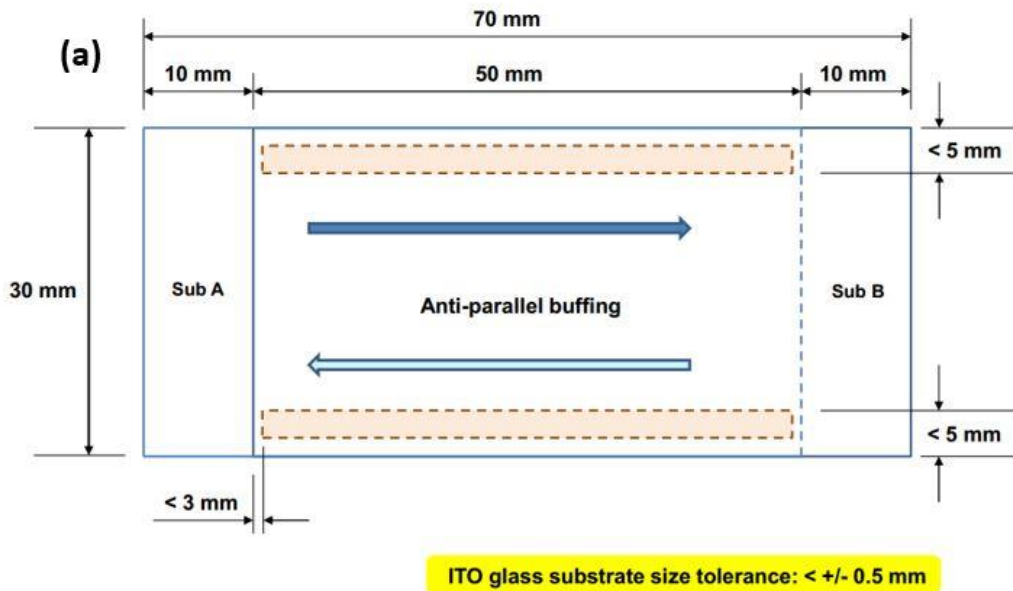


Figure 3-2: (a-c) Sequence of steps involved in phase transferring of AuNRs.

Initially, 100mg of thiol terminated polystyrene was measured and dissolved in 4ml of THF. 2ml of AuNR solution was taken in a new 20ml vial. To this AuNR solution, 1ml of polystyrene/THF solution was added and shaken vigorously. Because of the hydrophobic interaction, the nanorods stick the walls of the vial and the residual solution at the bottom becomes clear. This mixture was allowed to settle was for 15 minutes. The clear solution of THF at the bottom of the vial was pipetted out carefully. Depending on the desired concentration of the AuNRs, 2 to 5ml of toluene was added. The vial was shaken and sonicated to homogenously disperse the rods in the solution for further use in dielectric studies and the AuNR concentration was kept at an optical density of ~ 1 for all three aspect ratios and used as is.⁶⁰

3.2 Dielectric Anisotropy and Spectroscopy Measurements

Field aligned carbon nanotubes in dilute suspensions have been studied but the orientation order of AuNRs have not been studied from the dielectric standpoint. The following experiments were an effort to bridge the theory and experiment to yield quantitative measurement of orientational parameter at different voltages and frequency. For this study, we could not use the existing Instec LC cells or IPS LC cells as the limited ITO region in these cells give rise to edge effect where the buckling electric field lines lead to huge gradient pulling away all the AuNRs towards itself. Therefore, we had to design a custom cells (from Instec Inc) that had complete coverage of the longitudinal surface with ITO coating and thereby eliminating the edge effect. The schematic and actual image of the cell is presented in the following image. The custom cells were made to specific dimensions and the thickness varied from 5 μm , 10 μm and 20 μm . The cells did have polyimide anti-parallel buffing to minimize the possibility of shorting the cells by AuNRs forming a conductive pathway.



(b)

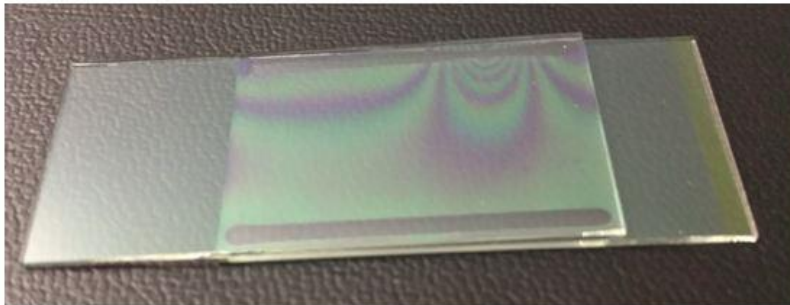


Figure 3-3: (a) Schematic of the custom designed ITO cell with dimensions.

(b) Actual image of the cell used.

Considering AuNRs to be a prolate spheroid (with semi-major axis length a , and two semi-minor axes b and c of equal length), one can deduce that longitudinal polarizability (α_{\parallel}) along the major axis of the nanorods to be distinctly different from the transverse polarizability tensor (α_{\perp}). The alignment of AuNRs within a cell under external field can be schematically shown as follows.

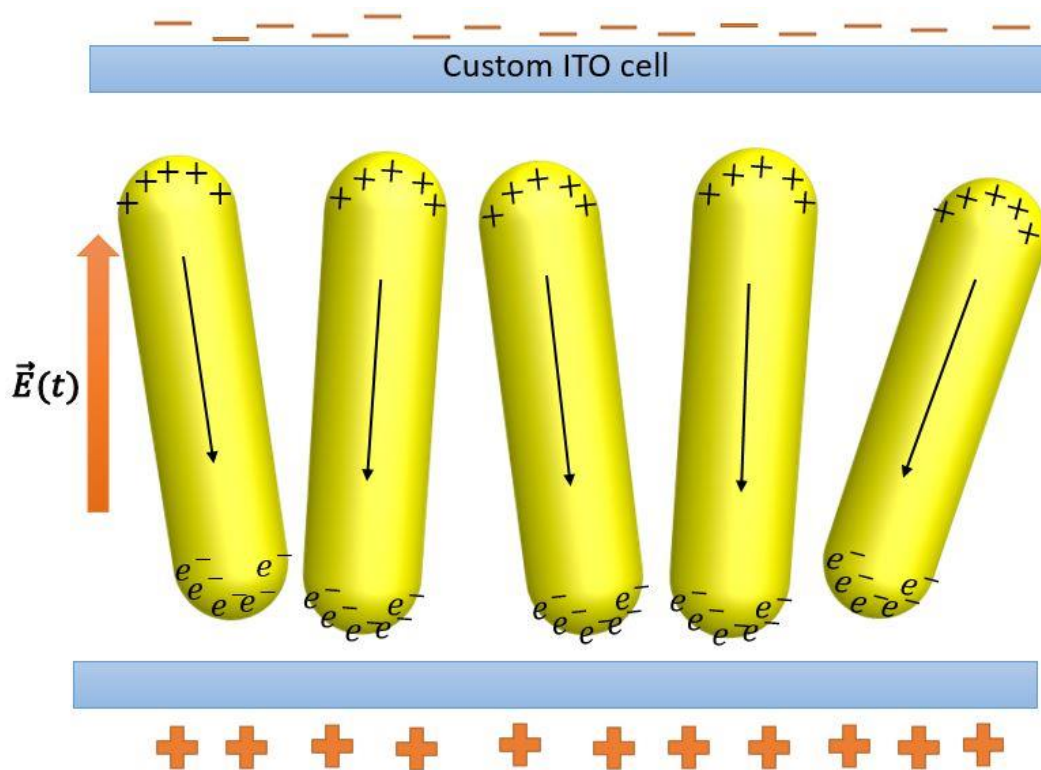


Figure 3-4: Schematic illustrating the induced dipole in AuNRs within a ITO cell, under the applied electric field

Under an applied field, induced dipoles moments are created within the rods and this is given by the following expression, where $\bar{\alpha}_o$ is the polarizability tensor of the nanorods.

$$\vec{p} = \bar{\alpha}_o \vec{E}(t)$$

The electric field induced ordering of AuNRs is a result of the torque that the external field exerts on the rods and this torque is represented by this following equation 3-1.

$$\begin{aligned}\vec{T}(\theta, t) &= (\overline{\alpha}_o \vec{E}(t)) \times \vec{E}(t) \\ &= -\Delta\alpha_o \cos(\theta) \sin(\theta) E^2(t) \hat{3}\end{aligned}$$

Equation 3-2

Where, \vec{p} is the dipole moment, $\overline{\alpha}_o$ is the polarizability tensor as stated before, $\vec{E}(t)$ is the applied electric field, Θ = angle between the nanorod and the electric field and $\Delta\alpha_o$ is the difference in longitudinal & transverse polarizability tensor.^{61,62} The physics behind the derivation of this equation is beyond the scope of this work.

3.3 Quantitative Measurement of Dielectric Anisotropy

For the purpose of measuring the dielectric anisotropy of AuNRs, we used the same setup used in the previous study involving FNPs i.e., automatic liquid crystal tester and signal generator coupled to a lock-in amplifier. The orientational order not only depends on the applied field but also on the depolarization anisotropy and nanorods volume.[x] The concentration of phase transferred nanorods were adjusted a OD of 1 in solvents such as toluene and RI oil. Using a micropipette, a small fraction of these suspension was

introduced into 5μ ITO cell at room temperature and annealed for 5 minutes. The voltage across the cells was slowly raised in steps 0.5V until we reached the limit for that particular cell thickness. The capacitance of the ITO cell in comparison to empty cell capacitance and dielectric constant were calculated and plotted against the root mean squared voltage across the cell (Figure 3-5)

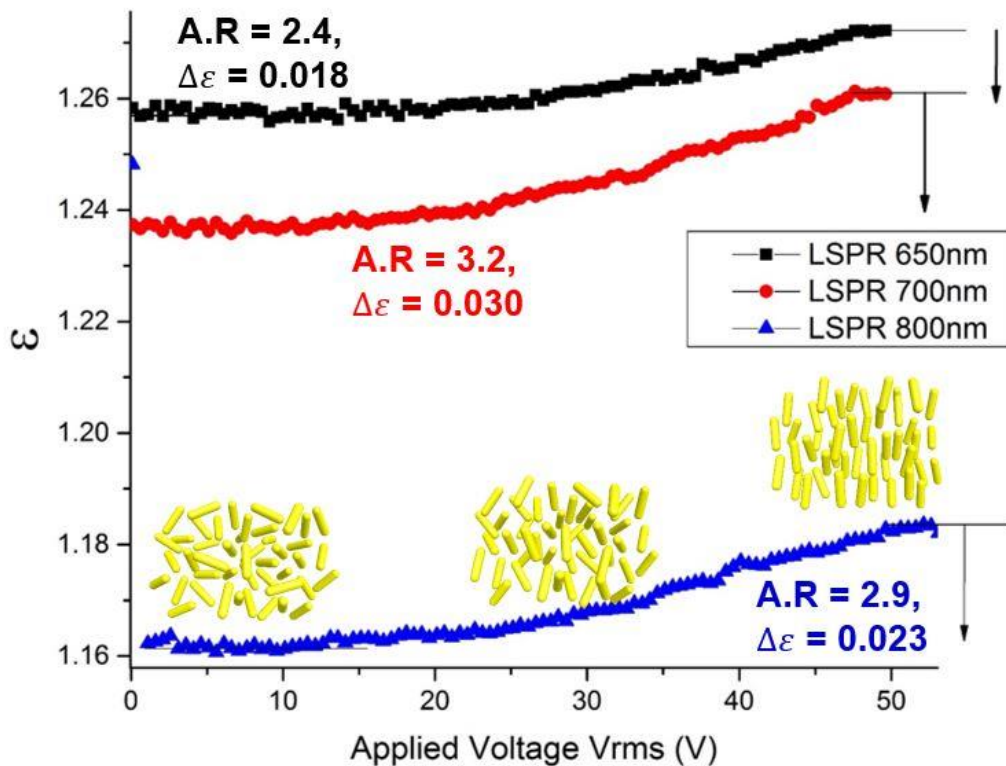


Figure 3-5 : Change in dielectric constant as a function of applied electric field for 5μ cell has been plotted. Dielectric constant increases with voltage.

The threshold voltage at which the slope of the above curve starts rising from the plateau is noted and the difference in dielectric constant at this threshold voltage and the

highest voltage is considered as the anisotropy and it qualitatively indicates the orientational order of the nanorods. The depolarization tensor which is responsible for the mechanical torque is directly related to the aspect ratio and the volume of each rod. So, the experimental results complies with this hypothesis i.e., higher aspect ratio AuNRs show higher dielectric anisotropy compared and this has been shown in the image below.

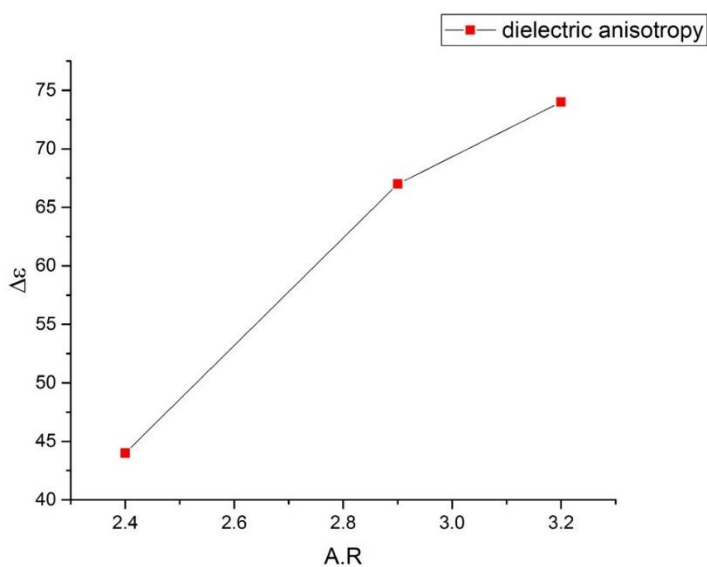


Figure 3-6: Dielectric anisotropy as a function of aspect ratio of the nanorods

From our preliminary studies it suffices to say that, AuNRs can be aligned via electric fields in non-polar solvents and the critical field needed to align bulk of the rods depends on the volume of individual rods, aspect ratio, spacing of the cells used for measurement and the solvent used. To make a conclusive statement further tests and trial runs for various concentrations and aspect ratios must be conducted.

3.4 Dielectric Spectroscopy

Understanding the frequency dependence of these nanorods suspensions is critical for usage in devices, achieve high efficiency and in possible metamaterial applications. Towards this end, we attempted to study the real and imaginary components of the dielectric constant using spectroscopic techniques. As outlined in chapter 1, there are many different dominant modes of relaxation and to characterize the storage and loss factor in wide frequency regimes, we employed two different high-resolution spectrometers i.e., Keysight E4980A for frequencies up to 10^6 Hz and E4982A LCR for frequencies between 10^6 Hz - 10^{12} Hz. Because of the limited time constraints, we were able to run few different trials in two different non-polar solvents i.e., toluene and R.I matched silicon oil. The figure below has both real and imaginary components of the complex dielectric constant as a function of frequency for a cell containing AuNRs of aspect ratio 3.2 and in R.I oil. It is important to note that following data applies to the longitudinal, complex dielectric constant of the nanorods.⁶³

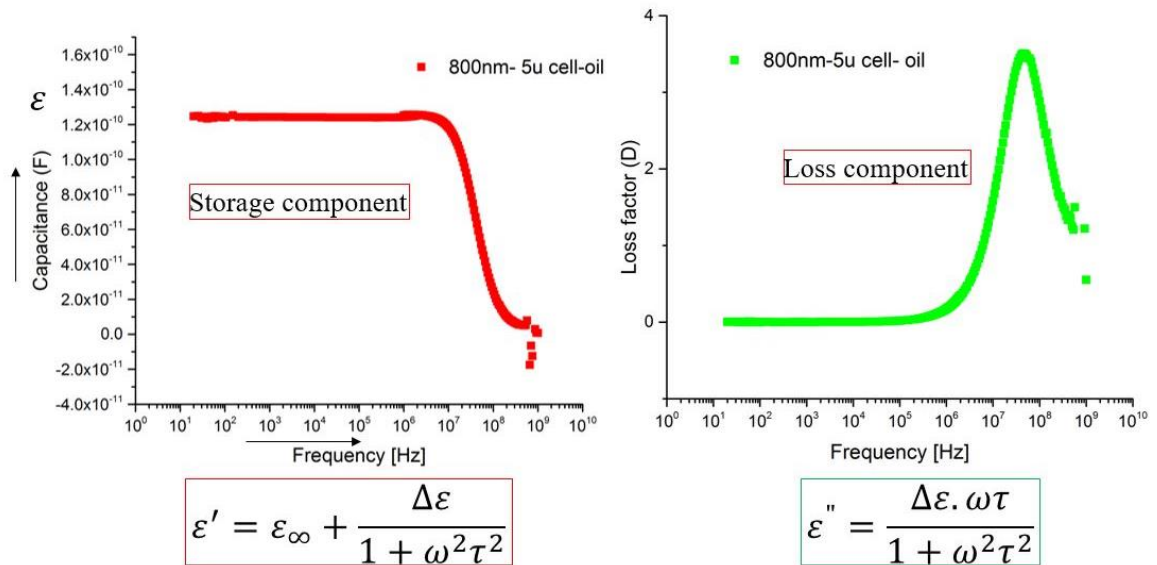


Figure 3-7: (left) Real component indicating the storage factor. (Right) Imaginary component of complex dielectric constant indicating the loss factor.

Another attempt to study the same but using toluene as solvent did exhibit similar spectral characteristics but there was a distinct contribution from the chemical structure of toluene and for this reason, we decided not to proceed with toluene for dielectric spectroscopy measurements. The following figure has a lot of real and imaginary parts of the spectra for AuNRs with aspect ratio of 2.4 and dispersed in toluene. The cell used for this test had a thickness of $20\mu\text{m}$ and the voltage was kept to a minimum of 1V.

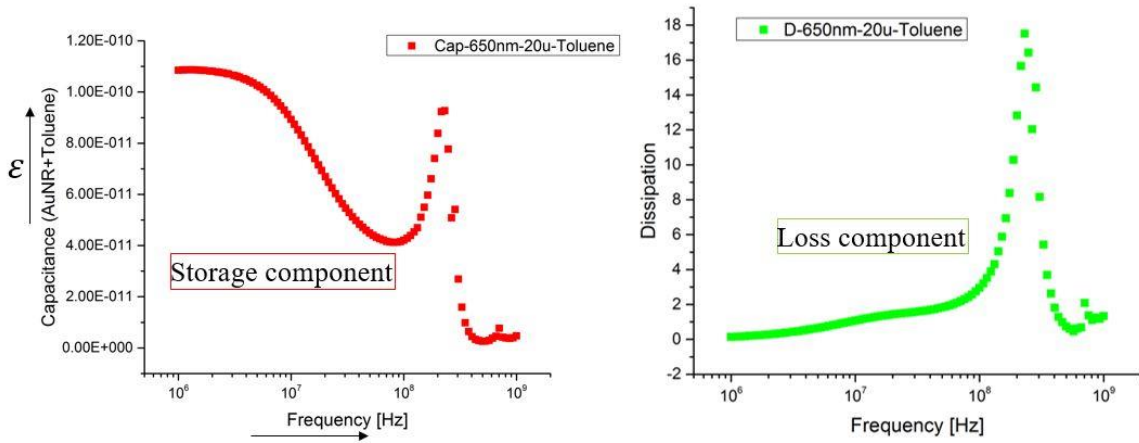


Figure 3-8: Dielectric relaxation spectra of AuNRs dispersed in toluene. One can observe the distinct peak from the toluene chemical structure in both real and imaginary components.

It is also a major challenge to separate the contribution of the solvent medium from the AuNRs itself when it comes to relaxation dynamics. We found that the refractive index matched silicon oil produces very similar relaxation dynamics (Figure 3-9) as shown in Figure 3-7 and for this reason, it is essential to continue this study with higher concentration suspensions to differentiate the effects of the solvent from the rods.

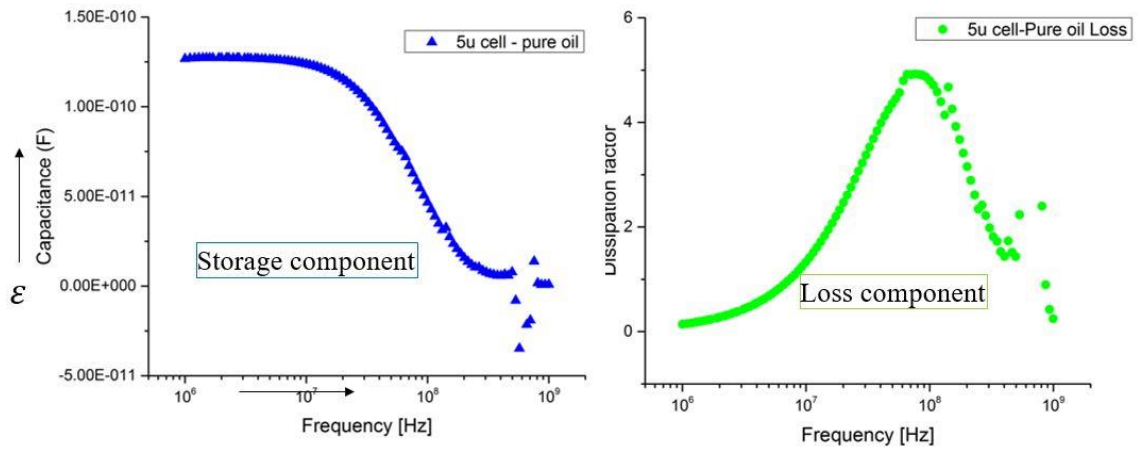


Figure 3-9: Dielectric relaxation spectra of pure R.I oil as a function of frequency in a 5 μ m cell.

Further investigation along this line of work could elucidate on the critical field characteristics and loss behavior for different aspect ratio of AuNRs at various concentrations. Thereby, one would be able to optimize the efficiency by choosing a certain window of concentration and aspect ratio which would correspond to faster switching times and alignment.

Chapter 4

Perspective and Future Work

Some of the most widely studied systems like ferroelectric polymers, amphiphilic polymers can be used in conjunction with nanoparticles to discover new electro-optical effects, decrease rotational viscosity and ionic conductivity. We envisage that future studies in this direction would be interesting to unearth new effects.

4.1 Ionic Conductivity in Doped LCs

The surface of nanoparticles, defects in the LC media and polymer ligands or the polymer corona on the surface of functionalized nanoparticles are all considered potential charge trapping sites. As shown in the image below,

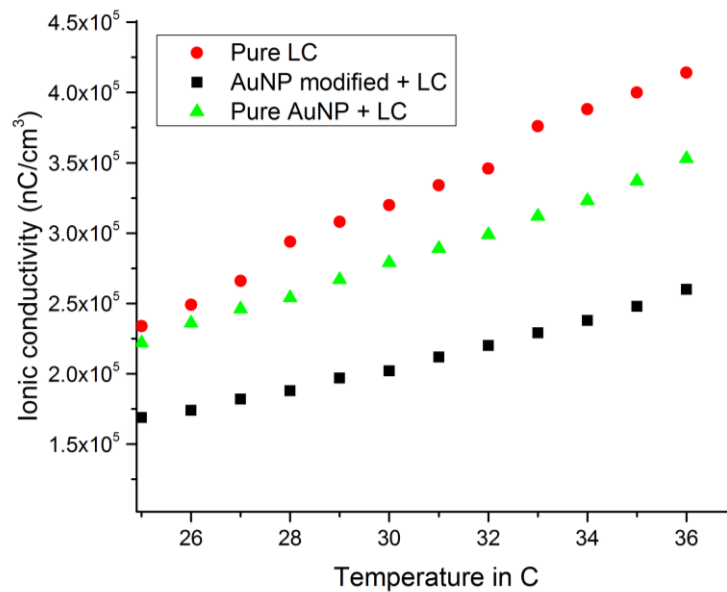


Figure 4-1: Ionic conductivity of LC when doped with functionalized AuNPs

We functionalized 20nm, 0.2 wt% AuNPs with PEO₄₅-b-PS₆₇₀-SH polymer and were used to dope 5CB LC in nematic phase. We found that modified LCs exhibit significantly low ionic conductivity and low ionic conductivity in LCs account for faster switching and such doping methods could potentially lead to more efficient displays.

4.2 Ferroelectric Polymers in LCs

Polyvinylidene fluoride (PVDF) is a well-known ferroelectric polymer (FPs) that has been used for supercapacitor applications. Until now, there has been no reports about the effects of doping FPs in LCs. FPs tend to phase separate in LCs but it is possible to attach nematic soluble polystyrene block. Our preliminary test involving a isotropic sample of 5CB doped with 0.025 wt% PVDF did show observable hysteresis.

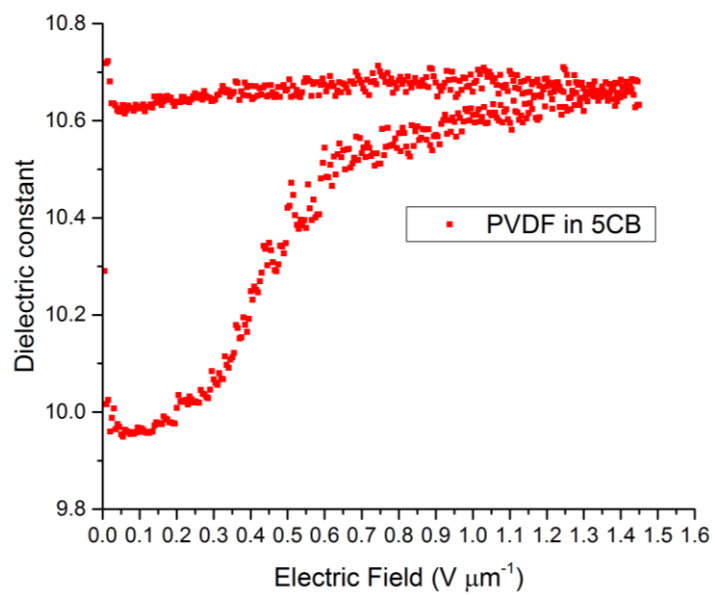


Figure 4-2: Hysteresis observed in PVDF doped 5CB in isotropic phase

4.3 Conclusions

Several significant conclusions can be drawn from these two works.

First, LCs can be aligned into a domain even in isotropic phase via doping of nanoparticles and doping nematic 5CB with BaTiO₃ FNPs in small quantities facilitate the formation of pseudonematic domains that is particularly pronounced in the isotropic phase of LCs. Polymer functionalization of FNPs enable enhanced volume of these pseudonematic domains and can be locked in space for a very long time. We infer that polymer ligands play a crucial role in providing a scaffold-like structure and aligning the mesogens via pi-pi bond stacking. One could also deduce that by using such polymer functionalization, non-volatile memory devices could be created for actual applications.

Second, AuNRs tend to align in electric field and the efficacy depends on the aspect ratio, solvent chemistry and volume of individual nanorods. Aligned nanorods affect the overall dielectric capacitance of the system and can be detected by dielectric techniques. Display devices using anisotropic nanoparticles like AuNRs could potentially have faster switching than LC mesogens owing to stronger coupling with electric fields and reversal via thermal perturbations. In a population of mixed aspect ratio AuNRs, each segment of rods with similar aspect ratio can be tuned separately.

Appendix A

X-ray Diffraction pattern of BaTiO₃

Barium Titanate (Barium Titanium Oxide, BaTiO₃) Nanoparticles, X-ray for 50nm, Stock#: US3835

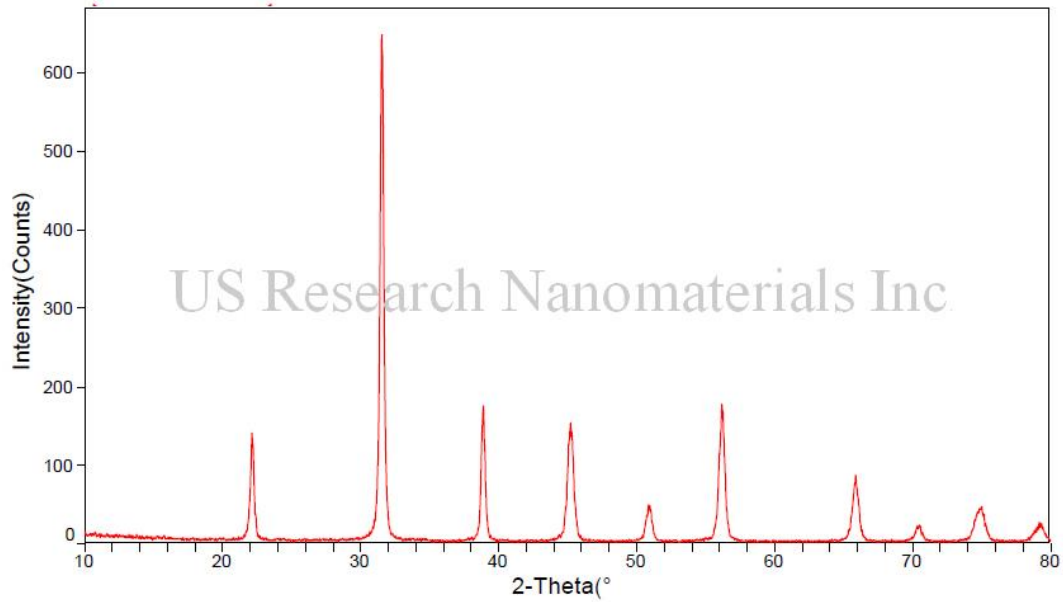


Figure 0-1: XRD spectra indicating the single phase of BaTiO₃ nanoparticles
(Courtesy of U.S Nanomaterials Research Inc.)

The peak seen here clearly indicates the single phase of BaTiO₃ FNP's and if the material was amorphous, we would not be seeing this distinct peak.

Appendix B

Dielectric Spectroscopy setup

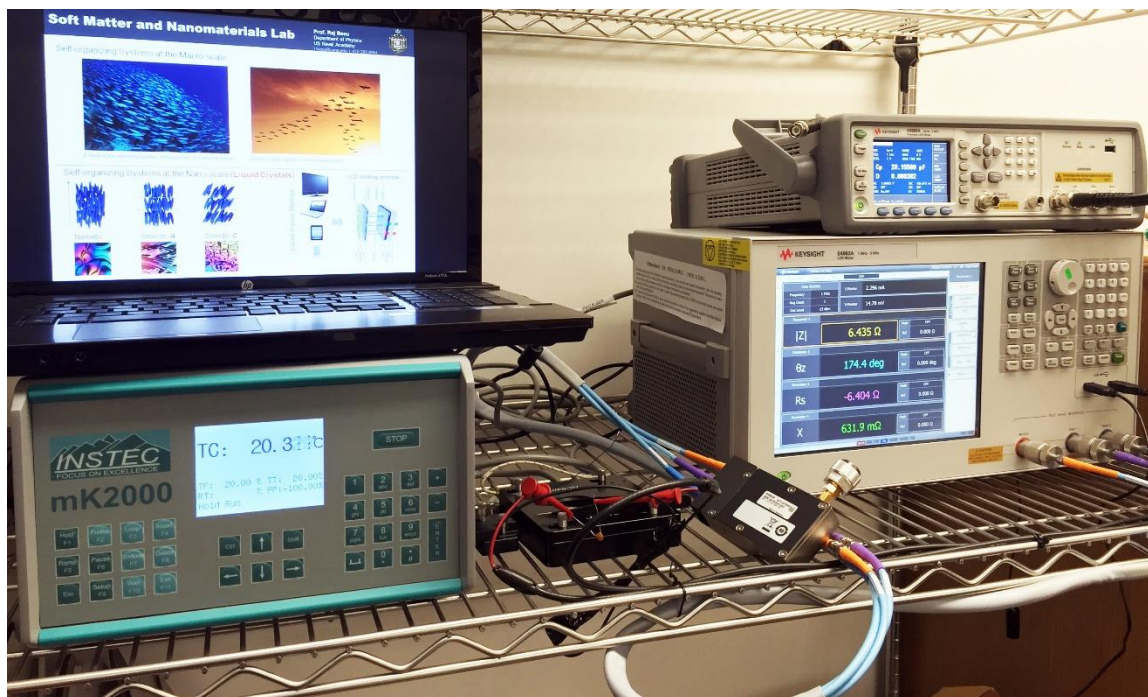


Figure 0-1: Keysight E4980A and E4982A broadband frequency spectrometers.

References

1. Kao, K. C., 2 - Electric Polarization and Relaxation. In *Dielectric Phenomena in Solids*, Academic Press: San Diego, 2004; pp 41-114.
2. Kremer, F.; Schonhals, A., *Broadband Dielectric Spectroscopy*. Springer: 2003.
3. Jonscher, A. K., Dielectric relaxation in solids. *Journal of Physics D: Applied Physics* **1999**, 32 (14), R57.
4. Kao, K. C., 3 - Optical and Electro-Optic Processes. In *Dielectric Phenomena in Solids*, Academic Press: San Diego, 2004; pp 115-212.
5. Runt, J. P.; Fitzgerald, J. J., *Dielectric spectroscopy of polymeric materials*. American Chemical Society: 1997.
6. Khatua, S.; Manna, P.; Chang, W.; Tcherniak, A.; Friedlander, E.; Zubarev, E.; Link, S., Plasmonic Nanoparticles-Liquid Crystal Composites. *Journal of Physical Chemistry C* **2010**, 114 (16), 7251-7257.
7. Stamatoiu, O.; Mirzaei, J.; Feng, X.; Hegmann, T., Nanoparticles in Liquid Crystals and Liquid Crystalline Nanoparticles. *Liquid Crystals: Materials Design and Self-Assembly* **2012**, 318, 331-393.
8. Hegmann, T.; Qi, H.; Marx, V., Nanoparticles in liquid crystals: Synthesis, self-assembly, defect formation and potential applications. *Journal of Inorganic and Organometallic Polymers and Materials* **2007**, 17 (3), 483-508.
9. Lapanik, A.; Rudzki, A.; Kinkead, B.; Qi, H.; Hegmann, T.; Haase, W., Electrooptical and dielectric properties of alkylthiol-capped gold nanoparticle-ferroelectric liquid crystal nanocomposites: influence of chain length and tethered liquid crystal functional groups. *Soft Matter* **2012**, 8 (33), 8722-8728.
10. Basu, R., Soft memory in a ferroelectric nanoparticle-doped liquid crystal. *Physical Review E* **2014**, 89 (2).
11. Demus, D.; Goodby, J. W.; Gray, G. W.; Spiess, H. W.; Vill, V., *Handbook of Liquid Crystals, Low Molecular Weight Liquid Crystals I: Calamitic Liquid Crystals*. John Wiley & Sons: 2011.
12. Prost, J., *The physics of liquid crystals*. Oxford university press: 1995.
13. Aliev, F.; Nazario, Z.; Sinha, G., Broadband dielectric spectroscopy of confined liquid crystals. *Journal of Non-Crystalline Solids* **2002**, 305 (1-3), 218-225.

14. Zhang, Y.; Liu, Q.; Mundoor, H.; Yuan, Y.; Smalyukh, I. I., Metal nanoparticle dispersion, alignment, and assembly in nematic liquid crystals for applications in switchable plasmonic color filters and E-polarizers. *ACS Nano* **2015**, *9* (3), 3097-108.
15. Kumar, A.; Singh, G.; Joshi, T.; Rao, G. K.; Singh, A. K.; Biradar, A. M., Tailoring of electro-optical properties of ferroelectric liquid crystals by doping Pd nanoparticles. *Applied Physics Letters* **2012**, *100* (5).
16. Lorenz, A.; Zimmermann, N.; Kumar, S.; Evans, D. R.; Cook, G.; Martinez, M. F.; Kitzerow, H.-S., Doping a Mixture of Two Smectogenic Liquid Crystals with Barium Titanate Nanoparticles. *Journal of Physical Chemistry B* **2013**, *117* (3), 937-941.
17. Liu, Q.; Cui, Y.; Gardner, D.; Li, X.; He, S.; Smalyukh, I. I., Self-Alignment of Plasmonic Gold Nanorods in Reconfigurable Anisotropic Fluids for Tunable Bulk Metamaterial Applications. *Nano Letters* **2010**, *10* (4), 1347-1353.
18. Kim, P.; Jones, S. C.; Hotchkiss, P. J.; Haddock, J. N.; Kippelen, B.; Marder, S. R.; Perry, J. W., Phosphonic acid-modified barium titanate polymer nanocomposites with high permittivity and dielectric strength. *Advanced Materials* **2007**, *19* (7), 1001-1005.
19. Paniagua, S. A.; Kim, Y.; Henry, K.; Kumar, R.; Perry, J. W.; Marder, S. R., Surface-Initiated Polymerization from Barium Titanate Nanoparticles for Hybrid Dielectric Capacitors. *Acs Applied Materials & Interfaces* **2014**, *6* (5), 3477-3482.
20. Jiang, B.; Pang, X.; Li, B.; Lin, Z., Organic-Inorganic Nanocomposites via Placing Monodisperse Ferroelectric Nanocrystals in Direct and Permanent Contact with Ferroelectric Polymers. *Journal of the American Chemical Society* **2015**, *137* (36), 11760-11767.
21. Ouchi, Y.; Feller, M. B.; Moses, T.; Shen, Y. R., Surface memory effect at the liquid-crystal-polymer interface. *Phys Rev Lett* **1992**, *68* (20), 3040-3043.
22. Qi, H.; Hegmann, T., Impact of nanoscale particles and carbon nanotubes on current and future generations of liquid crystal displays. *Journal of Materials Chemistry* **2008**, *18* (28), 3288-3294.
23. Matharu, A. S.; Jeeva, S.; Ramanujam, P. S., Liquid crystals for holographic optical data storage. *Chem Soc Rev* **2007**, *36* (12), 1868-80.
24. Ikeda, T.; Tsutsumi, O., Optical switching and image storage by means of azobenzene liquid-crystal films. *Science* **1995**, *268* (5219), 1873-5.
25. Bisoyi, H. K.; Kumar, S., Liquid-crystal nanoscience: an emerging avenue of soft self-assembly. *Chem Soc Rev* **2011**, *40* (1), 306-19.

26. Feng, X.; Sosa-Vargas, L.; Umadevi, S.; Mori, T.; Shimizu, Y.; Hegmann, T., Discotic Liquid Crystal-Functionalized Gold Nanorods: 2-and 3D Self-Assembly and Macroscopic Alignment as well as Increased Charge Carrier Mobility in Hexagonal Columnar Liquid Crystal Hosts Affected by Molecular Packing and pi-pi Interactions. *Advanced Functional Materials* **2015**, *25* (8), 1180-1192.
27. Trivedi, R.; Klevets, I.; Senyuk, B.; Lee, T.; Smalyukh, I., Reconfigurable interactions and three-dimensional patterning of colloidal particles and defects in lamellar soft media. *Proceedings of the National Academy of Sciences of the United States of America* **2012**, *109* (13), 4744-4749.
28. Rodarte, A.; Pandolfi, R.; Ghosh, S.; Hirst, L., Quantum dot/liquid crystal composite materials: self-assembly driven by liquid crystal phase transition templating. *Journal of Materials Chemistry C* **2013**, *1* (35), 5527-5532.
29. Lavrentovich, O. D., Liquid crystals, photonic crystals, metamaterials, and transformation optics. *Proc Natl Acad Sci U S A* **2011**, *108* (13), 5143-4.
30. Gardner, D.; Evans, J.; Smalyukh, I., Towards Reconfigurable Optical Metamaterials: Colloidal Nanoparticle Self-Assembly and Self-Alignment in Liquid Crystals. *Molecular Crystals and Liquid Crystals* **2011**, *545*, 1227-1245.
31. Mühlig, S.; Rockstuhl, C.; Yannopapas, V.; Bürgi, T.; Shalkevich, N.; Lederer, F., Optical properties of a fabricated self-assembled bottom-up bulk metamaterial. *Optics Express* **2011**, *19* (10), 9607-9616.
32. Pratibha, R.; Park, K.; Smalyukh, I. I.; Park, W., Tunable optical metamaterial based on liquid crystal-gold nanosphere composite. *Opt Express* **2009**, *17* (22), 19459-69.
33. Acreman, A.; Kaczmarek, M.; D'Alessandro, G., Gold nanoparticle liquid crystal composites as a tunable nonlinear medium. *Physical Review E* **2014**, *90* (1).
34. Liu, Q. K.; Yuan, Y.; Smalyukh, II, Electrically and Optically Tunable Plasmonic Guest-Host Liquid Crystals with Long-Range Ordered Nanoparticles. *Nano Letters* **2014**, *14* (7), 4071-4077.
35. Reznikov, Y.; Buchnev, O.; Tereshchenko, O.; Reshetnyak, V.; Glushchenko, A.; West, J., Ferroelectric nematic suspension. *Applied Physics Letters* **2003**, *82* (12), 1917.
36. Haase, A. M. a. P. A. a. A. G. a. A. L. a. W., Complementary studies of BaTiO₃ nanoparticles suspended in a ferroelectric liquid-crystalline mixture. *EPL (Europhysics Letters)* **2009**, *87* (2), 27009.
37. Herrington, M. R.; Buchnev, O.; Kaczmarek, M.; Nandhakumar, I., The Effect of the Size of BaTiO₃ Nanoparticles on the Electro-Optic Properties of Nematic Liquid Crystals. *Molecular Crystals and Liquid Crystals* **2010**, *527*, 72-79.

38. Rudzki, A.; Evans, D. R.; Cook, G.; Haase, W., Size dependence of harvested BaTiO₃ nanoparticles on the electro-optic and dielectric properties of ferroelectric liquid crystal nanocolloids. *Applied Optics* **2013**, *52* (22), E6-E14.
39. Shukla, R. K.; Liebig, C. M.; Evans, D. R.; Haase, W., Electro-optical behaviour and dielectric dynamics of harvested ferroelectric LiNbO₃ nanoparticle-doped ferroelectric liquid crystal nanocolloids. *Rsc Advances* **2014**, *4* (36), 18529-18536.
40. Ganguly, P.; Kumar, A.; Tripathi, S.; Haranath, D.; Biradar, A. M., Faster and highly luminescent ferroelectric liquid crystal doped with ferroelectric BaTiO₃ nanoparticles. *Applied Physics Letters* **2013**, *102* (22), 222902.
41. Podoliak, N.; Buchnev, O.; Herrington, M.; Mavrona, E.; Kaczmarek, M.; Kanaras, A.; Stratakis, E.; Blach, J.; Henninot, J.; Warengem, M., Elastic constants, viscosity and response time in nematic liquid crystals doped with ferroelectric nanoparticles. *Rsc Advances* **2014**, *4* (86), 46068-46074.
42. Chiang, Y.; Chou, T.; Chao, C., Enhancement of electro-optical properties of twisted nematic liquid crystals by doping aromatic hydrocarbon liquids. *Optics Express* **2014**, *22* (25), 30882-30888.
43. Fujikake, H.; Murashige, T.; Jun, Y. N.; Kikuchi, H.; Kawakita, M.; Takizawa, K., Electrooptical properties of free-standing polymer-stabilized ferroelectric liquid crystal films. *Electronics and Communications in Japan Part Ii-Electronics* **2002**, *85* (5), 35-42.
44. Fujikake, H.; Murashige, T.; Sato, H.; Iino, Y.; Kikuchi, H.; Kawakita, M.; Tsuchiya, Y., Polymer-stabilized ferroelectric liquid crystal for flexible displays using plastic substrates. In *Liquid Crystals V*, Khoo, I. C., Ed. 2001; Vol. 4463, pp 71-78.
45. Ouyang, J.; Chu, C. W.; Szmada, C. R.; Ma, L.; Yang, Y., Programmable polymer thin film and non-volatile memory device. *Nat Mater* **2004**, *3* (12), 918-22.
46. Muševič, I.; Zumer, S., Liquid crystals: Maximizing memory. *Nat Mater* **2011**, *10* (4), 266-8.
47. Prakash, J.; Choudhary, A.; Kumar, A.; Mehta, D. S.; Biradar, A. M., Nonvolatile memory effect based on gold nanoparticles doped ferroelectric liquid crystal. *Applied Physics Letters* **2008**, *93* (11).
48. Basu, R.; Iannacchione, G. S., Dielectric hysteresis, relaxation dynamics, and nonvolatile memory effect in carbon nanotube dispersed liquid crystal. *Journal of Applied Physics* **2009**, *106* (12), 124312.

49. Marino, L.; Marino, S.; Wang, D.; Bruno, E.; Scaramuzza, N., Nonvolatile memory effects in an orthoconic smectic liquid crystal mixture doped with polymer-capped gold nanoparticles. *Soft Matter* **2014**, *10* (21), 3842-3849.
50. Musevic, I.; Skarabot, M.; Tkalec, U.; Ravnik, M.; Zumer, S., Two-dimensional nematic colloidal crystals self-assembled by topological defects. *Science* **2006**, *313* (5789), 954-958.
51. He, J.; Liu, Y.; Babu, T.; Wei, Z.; Nie, Z., Self-assembly of inorganic nanoparticle vesicles and tubules driven by tethered linear block copolymers. *J Am Chem Soc* **2012**, *134* (28), 11342-5.
52. Basu, R., Effect of carbon nanotubes on the field-induced nematic switching. *Applied Physics Letters* **2013**, *103* (24).
53. Jaffe, B.; Cook, W. R.; Jaffé, H. L. C., *Piezoelectric ceramics*. Academic Press: London, New York., 1971; p ix, 317 p.
54. Adam, C.; Clark, S.; Ackland, G.; Crain, J., Conformation-dependent dipoles of liquid crystal molecules and fragments from first principles. *Physical Review E* **1997**, *55* (5), 5641-5649.
55. Kim, P.; Doss, N. M.; Tillotson, J. P.; Hotchkiss, P. J.; Pan, M. J.; Marder, S. R.; Li, J. Y.; Calame, J. P.; Perry, J. W., High Energy Density Nanocomposites Based on Surface-Modified BaTiO₃ and a Ferroelectric Polymer. *Acs Nano* **2009**, *3* (9), 2581-2592.
56. Kirby, G.; Harris, D.; Li, Q.; Lewis, J., Poly(acrylic acid)-poly(ethylene oxide) comb polymer effects on BaTiO₃ nanoparticle suspension stability. *Journal of the American Ceramic Society* **2004**, *87* (2), 181-186. (56a) <http://press.ihs.com/press-release/technology/flat-panel-display-revenues-forecast-fall-2015-ihs-says>
57. Zijlstra, P.; Chon, J. W. M.; Gu, M., Five-dimensional optical recording mediated by surface plasmons in gold nanorods. *Nature* **2009**, *459* (7245), 410-413.
58. Fontana, J.; da Costa, G. K. B.; Pereira, J. M.; Naciri, J.; Ratna, B. R.; Palfy-Muhoray, P.; Carvalho, I. C. S., Electric field induced orientational order of gold nanorods in dilute organic suspensions. *Applied Physics Letters* **2016**, *108* (8), 081904.
59. Zheng, X.; Fontana, J.; Pevnyi, M.; Ignatenko, M.; Wang, S.; Vaia, R.; Palfy-Muhoray, P., The effects of nanoparticle shape and orientation on the low frequency dielectric properties of nanocomposites. *Journal of Materials Science* **2012**, *47* (12), 4914-4920.

60. Fontana, J.; Naciri, J.; Rendell, R.; Ratna, B. R., Macroscopic Self-Assembly and Optical Characterization of Nanoparticle–Ligand Metamaterials. *Advanced Optical Materials* **2013**, *1* (1), 100-106.
61. Thomas, M. R.; Hallett, J. E.; Klein, S.; Mann, S.; Perriman, A. W.; Richardson, R. M., Stability and Orientational Order of Gold Nanorods in Nematic Suspensions: A Small Angle X-ray Scattering Study. *Molecular Crystals and Liquid Crystals* **2015**, *610* (1), 44-50.
62. Zijlstra, P.; van Stee, M.; Verhart, N.; Gu, Z.; Orrit, M., Rotational diffusion and alignment of short gold nanorods in an external electric field. *Physical Chemistry Chemical Physics* **2012**, *14* (13), 4584-4588.
63. Ruijgrok, P. V.; Verhart, N. R.; Zijlstra, P.; Tchebotareva, A. L.; Orrit, M., Brownian fluctuations and heating of an optically aligned gold nanorod. *Physical review letters* **2011**, *107* (3), 037401.